Endosomal WASH and exocyst complexes control exocytosis of MT1-MMP at invadopodia

Pedro Monteiro,[1,2] Carine Rossé,[1,2] Antonio Castro-Castro,[1,2] Marie Irondelle,[1,2] Emilie Lagoutte,[1,2] Perrine Paul-Gilloteaux,[1,3] Claire Desnos,[4,5] Etienne Formstecher,[6] François Darchen,[4,5] David Perrais,[7,8] Alexis Gautreau,[9] Maud Hertzog,[1,2] and Philippe Chavrier[1,2]

[1]Research Center, Institut Curie, 75005 Paris, France
[2]Membrane and Cytoskeleton Dynamics and [3]Cell and Tissue Imaging Facility, Centre National de la Recherche Scientifique UMR 144, 75005 Paris, France
[4]Université Paris Descartes and [5]Centre National de la Recherche Scientifique, UMR8192, 75006 Paris, France
[6]Hybrigenics services SAS, 75014 Paris, France
[7]University of Bordeaux and [8]Centre National de la Recherche Scientifique, Interdisciplinary Institute for Neuroscience, UMR 5297, 33000 Bordeaux, France
[9]Laboratoire d'Enzymologie et Biochimie Structurales, Centre National de la Recherche Scientifique UPR3082, 91198 Gif-sur-Yvette, France

Remodeling of the extracellular matrix by carcinoma cells during metastatic dissemination requires formation of actin-based protrusions of the plasma membrane called invadopodia, where the trans-membrane type 1 matrix metalloproteinase (MT1-MMP) accumulates. Here, we describe an interaction between the exocyst complex and the endosomal Arp2/3 activator Wiskott-Aldrich syndrome protein and Scar homolog (WASH) on MT1-MMP–containing late endosomes in invasive breast carcinoma cells. We found that WASH and exocyst are required for matrix degradation by an exocytic mechanism that involves tubular connections between MT1-MMP–positive late endosomes and the plasma membrane in contact with the matrix. This ensures focal delivery of MT1-MMP and supports pericellular matrix degradation and tumor cell invasion into different pathologically relevant matrix environments. Our data suggest a general mechanism used by tumor cells to breach the basement membrane and for invasive migration through fibrous collagen-enriched tissues surrounding the tumor.

Introduction

The matrix-degrading protrusions of the plasma membrane known as invadopodia are currently thought to form in invasive tumor cells when the extracellular matrix and cues from the tumor microenvironment, such as growth factors, trigger the assembly of F-actin into precursor structures through a signaling cascade involving Cdc42 and Nck1 and the actin regulatory proteins neuronal Wiskott-Aldrich syndrome protein (N-WASP), Arp2/3 complex, cortactin, and cofilin (Lorenz et al., 2004; Yamaguchi et al., 2005; Clark et al., 2007; Ayala et al., 2008; Oser et al., 2009, 2010; Murphy and Courtneidge, 2011). These precursors then mature into functional invadopodia upon accumulation of the trans-membrane type 1 matrix metalloproteinase (MT1-MMP; Artym et al., 2006; Clark et al., 2007; Sakurai-Yageta et al., 2008; Yu et al., 2012).

Correspondence to Philippe Chavrier: philippe.chavrier@curie.fr

M. Hertzog's present address is Centre National de la Recherche Scientifique, UMR 5100, Université Paul Sabatier, 31062 Toulouse, France.

Abbreviations used in this paper: CCD, charge-coupled device; MT1-MMP, membrane type 1 matrix metalloproteinase; N-WASP, neuronal Wiskott-Aldrich syndrome protein; SIM, structured illumination microscopy; TIRFM, total interference reflection fluorescence microscope; VAMP7, vesicle-associated membrane protein 7; WASH, Wiskott-Aldrich syndrome protein and Scar homolog.

A significant fraction of MT1-MMP is internalized from the cell surface as a means to regulate its surface level (Jiang et al., 2001; Uekita et al., 2001); In MDA-MB-231 human breast adenocarcinoma cells, we found the majority of intracellular MT1-MMP located in a late endosome compartment (Steffen et al., 2008). We and others reported that an exocytic machinery comprising cortactin, the vesicle-docking exocyst complex, and the SNARE protein vesicle-associated membrane protein 7 (VAMP7) is required for MT1-MMP delivery to invadopodia and invadopodia activity in tumor cells cultured on cross-linked gelatin as a matrix (Artym et al., 2006; Clark et al., 2007; Sakurai-Yageta et al., 2008; Steffen et al., 2008; Liu et al., 2009; Williams and Coppolino, 2011). Based on these findings, we proposed that this cohort of proteins regulates the trafficking and exocytosis of MT1-MMP from late endocytic storage compartments to its invadopodial target plasma membrane (Poincloux et al., 2009). However, the nature of the carriers that mediate plasma membrane

The Rockefeller University Press $30.00
J. Cell Biol. Vol. 203 No. 6 1063–1079
www.jcb.org/cgi/doi/10.1083/jcb.201306162

delivery of MT1-MMP, the mechanism underlying MT1-MMP exocytosis in the biogenesis of invadopodia, and how exocytosis is possibly influenced by the composition and biophysical properties of the matrix remain poorly understood.

Recent studies have documented an essential role for actin cytoskeleton dynamics in endosome function (Derivery et al., 2009; Gomez and Billadeau, 2009; Morel et al., 2009; Puthenveedu et al., 2010; Carnell et al., 2011; Harrington et al., 2011). The mechanism emerging from these on-going studies indicates that actin–Arp2/3 assemblies organize early endosomal membranes into functional subdomains and contribute to cargo sorting and generation of transport intermediates. Some of these studies also highlighted the essential role of the newly identified Wiskott-Aldrich syndrome protein and Scar homolog (WASH) complex, a member of the WASP (Wiskott–Aldrich syndrome protein) family of Arp2/3 activators associated with the endosomal/lysosomal system and playing a major role in the polymerization of endosomal actin (Derivery et al., 2009; Gomez and Billadeau, 2009; Duleh and Welch, 2010). All together, these data support a critical role for WASH in linking Arp2/3 and F-actin–assisted elongation and fission of endosomal tubules with sorting and trafficking from the endosomal system to the cell surface (Derivery et al., 2009; Gomez and Billadeau, 2009; Puthenveedu et al., 2010; Carnell et al., 2011; Temkin et al., 2011; Zech et al., 2011; Gomez et al., 2012). Here, we describe a novel interaction of WASH with the exocyst complex on MT1-MMP–containing late endosomes in invasive breast tumor cells. Our data support a mechanism of exocytosis of MT1-MMP through late endosome-to-plasma membrane connections occurring at invadopodia and requiring WASH and exocyst complexes for their formation.

Results

WASH and the exocyst complex interact on MT1-MMP–positive endosomes in breast tumor cells

In a series of yeast two-hybrid screens aimed at isolating partners of the eight subunits of the exocyst complex, we identified interactions of both Exo84 and Sec3 exocyst subunits with the amino-terminal region of WASH. Overlapping regions from independent isolated clones defined WASH domains interacting with Sec3 (amino acids 9–109 of WASH) or with Exo84 (amino acids 15–258 of WASH; unpublished data). By using fluorescence microscopy of MDA-MB-231 cells overexpressing GFP-WASH and immunofluorescence microscopy of the endogenous protein and in agreement with the function of WASH as an activator of the Arp2/3 complex (Derivery et al., 2009; Gomez and Billadeau, 2009; Duleh and Welch, 2010), we observed WASH puncta closely associated with punctate accumulations of Arp2/3 complex, F-actin, and the F-actin–binding protein cortactin on MT1-MMP–positive endosomes (Fig. S1 A and Fig. 1, A and B). Exo84 was also detected as puncta closely apposed to and partially overlapping with WASH and cortactin-positive subdomains on MT1-MMP–containing endosomes (Fig. 1, C and D; and Fig. S1 B). Live-cell imaging revealed highly dynamic WASH puncta associated with cortactin (Video 1). The number of WASH-cortactin patches seemed to correlate with endosome size (Fig. 1 B; Gomez and Billadeau, 2009; Derivery et al., 2012). Endosomal puncta of WASH and cortactin were more closely associated (mean distance of ∼2 pixels) as compared with WASH and Exo84-positive ones (∼5 pixels; Fig. 1 E). Similarly, we observed another component of the WASH complex, FAM21, associated with cortactin domains on MT1-MMP–positive endosomes (Fig. S1 C). WASH was also apposed to punctate structures containing the late endocytic SNARE protein VAMP7 on the limiting membrane of these endosomes (Fig. S1 D), in agreement with the predominant localization of MT1-MMP to late endosomes (Steffen et al., 2008; Williams and Coppolino, 2011). WASH- and cortactin-positive puncta were similarly associated with MT1-MMP–containing endosomes in BT-549 breast cancer cells (Fig. S1 E). To further evaluate association of WASH with cortactin or Exo84 on MT1-MMP–containing endosomes, we performed a Duolink in situ proximity ligation assay (Söderberg et al., 2006). This analysis confirmed a strong association between WASH and cortactin and a weaker one between WASH and Exo84, with most of the Duolink signal coinciding with MT1-MMP–containing endosomes (Fig. 1, F and G). Finally, endogenous WASH protein in HeLa cell extracts coimmunoprecipitated with overexpressed full-length Exo84 and Sec3 and with endogenous Sec8 (Fig. 1 H), thus confirming the two-hybrid results and showing that WASH interacts with the exocyst complex in vivo. Together, these findings reveal the existence of WASH- and Arp2/3–F-actin–cortactin–positive domains on MT1-MMP–containing late endosomes. The exocyst complex is closely apposed to and interacts with WASH-positive subdomains on MT1-MMP–positive endosomes, suggesting a coordinated function of these complexes in breast tumor cells.

WASH and exocyst control actin assembly on MT1-MMP–positive endosomes

To investigate the roles of WASH and the exocyst complex we first looked at the morphology of MT1-MMP–positive endosomes in MDA-MB-231 cells silenced for WASH or Exo84 with two independent siRNAs (Fig. S2, A and B). As previously reported (Steffen et al., 2008), MT1-MMP accumulated in large vacuolar compartments in the central region of the cell as well as in smaller vesicles spread throughout the cytoplasm (Fig. 2 A, class #1). Silencing of WASH resulted in drastic changes in the morphology of the MT1-MMP–containing endosomes: in ∼60% of cells they aggregated in the center (Fig. 2, A and B, class #2) and in ∼15% of them large clumps of MT1-MMP–positive structures appeared (Fig. 2, A and B, class #3). We observed a similar, albeit less marked, phenomenon in cells silenced for Exo84 (Fig. 2, A and B). Live-cell imaging revealed perinuclear aggregated MT1-MMP–positive endosomes in WASH-depleted cells, some with exaggerated tubular membrane extensions (Fig. 2 C and Video 2). This phenotype is reminiscent of endosome tubulation induced upon depletion of WASH seen in other cell types (Derivery et al., 2009; Gomez and Billadeau, 2009; Gomez et al., 2012). Given the proposed function of WASH-dependent actin/cortactin assembly in regulation of endosomal tubule dynamics, we explored the contribution of WASH and exocyst complex to the formation of Arp2/3–F-actin–cortactin punctate domains on MT1-MMP–positive late endosomes.

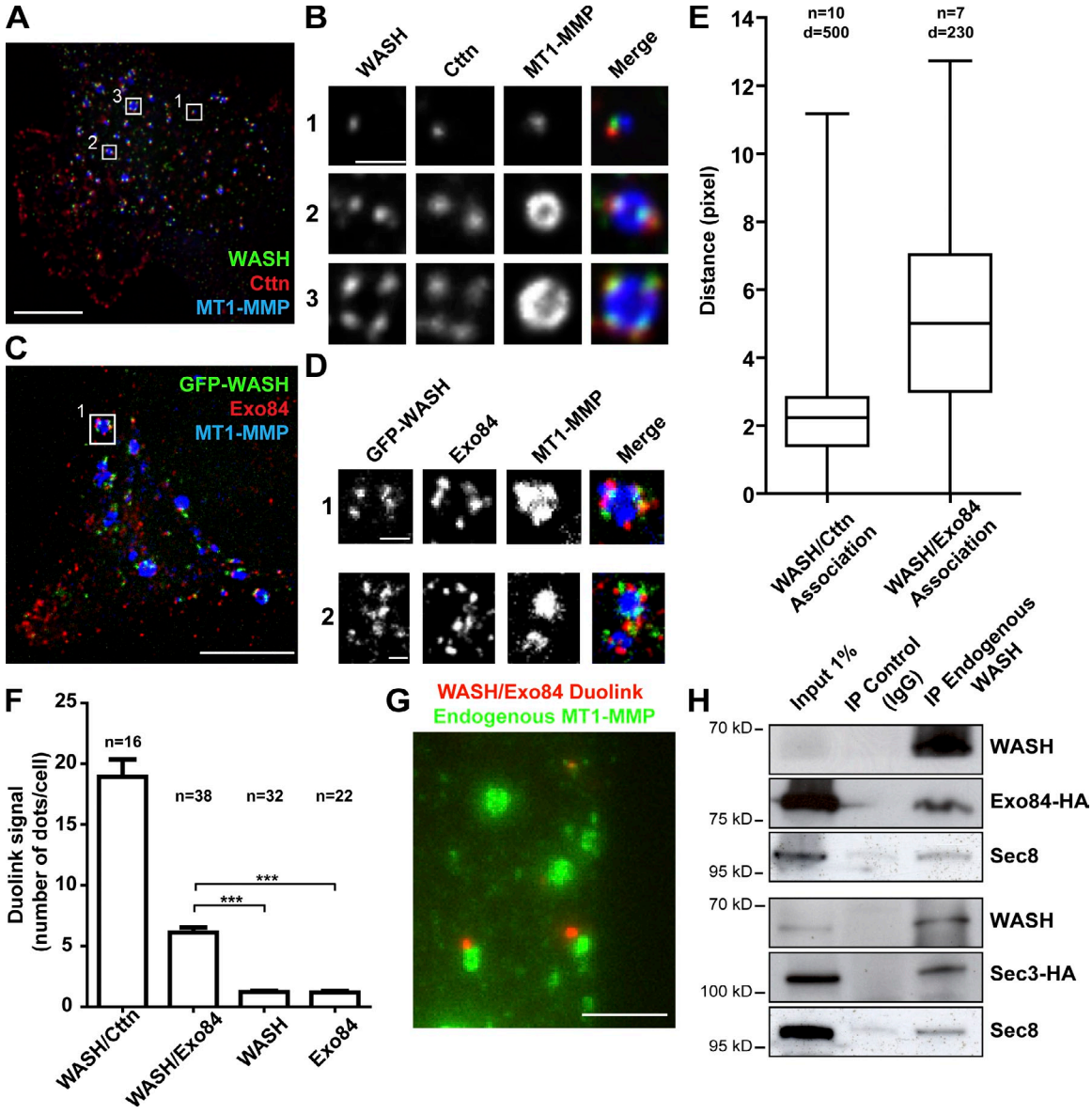

Figure 1. **WASH and exocyst complex associate on adjacent subdomains on MT1-MMP–positive endosomes.** (A) Association of endogenous WASH and cortactin (Cttn) on microdomains on MT1-MMPmCh–positive late endosomes. (B) Zoom of boxed regions in A. Images represent the middle plane of the cells. (C) MDA-MB-231 cells transfected with GFP-WASH were plated on cross-linked gelatin, stained for Exo84 and MT1-MMP, and imaged by 3D deconvolution microscopy. (D) Zoom of boxed region in C (box 1) and from another cell (box 2). Bars: (A and C) 5 µm; (B and D) 1 µm. (E) Box plots of the distance between adjacent puncta of WASH and cortactin or Exo84 on MT1-MMP–positive endosomes (in pixels). Whiskers show 25–75%. Numbers of cells (*n*) and of WASH-cortactin and WASH-Exo84 doublets (d) analyzed from independent experiments are indicated. (F) Quantification of Duolink dots using different antibody pairs as indicated (mean Duolink dots per cell ± SEM; *n* represents the number of cells analyzed for each condition). ***, $P < 0.001$ as compared with WASH-Exo84 combination. (G) Immunolabeling of MT1-MMP (green) was performed after the Duolink reaction between WASH and Exo84 antibodies (red dots). Bar, 5 µm. (H) Coimmunoprecipitation of exocyst subunits with WASH in HeLa cell lysates. Bound proteins were analyzed by immunoblotting with antibodies against WASH, HA-tag, and Sec8. Input lysates (1%) were loaded as control.

Silencing of WASH led to a large reduction of cortactin accumulation on endosomal compartments (Fig. 2, D and E). In contrast, silencing of N-WASP that is required for invadopodial actin assembly (Yamaguchi et al., 2005; Oser et al., 2009, 2010; Yu et al., 2012) had no effect on endosomal cortactin (and WASH)-positive microdomains (Fig. S3 C and Fig. 2, D and E). Interestingly, silencing of Exo84 was accompanied by a limited but significant increase of the size of WASH patches on MT1-MMP–positive endosomes and a marked lengthening of comet-shaped cortactin domains associated with WASH patches (Fig. 2, F and G). Similar observations were obtained upon depletion of Sec8 exocyst subunit (unpublished data). Together, these data indicate that WASH controls actin polymerization on MT1-MMP–positive endosomes and suggest that the exocyst complex associated with WASH may finely tune actin assembly required for regulation of endosomal membrane scission and remodeling (Derivery et al., 2009; Gomez and Billadeau, 2009; Park et al., 2013).

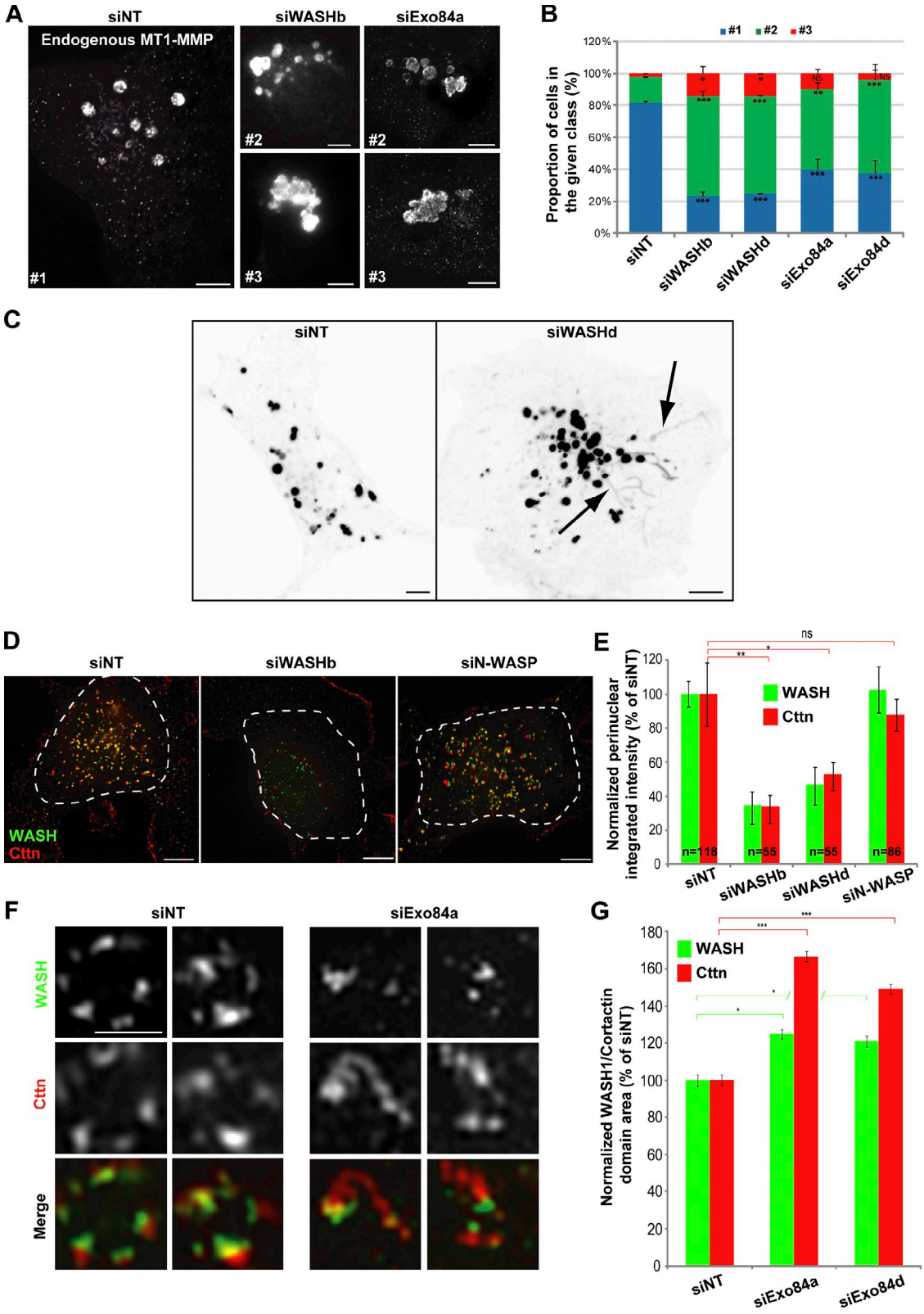

Figure 2. **Regulation of MT1-MMP–positive endosome dynamics by WASH and exocyst complex.** (A and B) MDA-MB-231 cells treated with the indicated siRNAs were plated on cross-linked gelatin and stained for endogenous MT1-MMP. Bars, 5 µm. Cells were scored according to the distribution of MT1-MMP–positive endosomes, i.e., normal distribution (#1, blue boxes in B), clustered endosomes (#2, green box), and aggregated endosomes (#3, red box). Values ploted in B are mean ± SEM of normalized endosome distribution from three independent experiments scoring ~100 cells for each siRNA. *, $P < 0.05$; **, $P < 0.01$; ***, $P < 0.001$ compared with siNT-treated cells (B). (C) MDA-MB-231 cells expressing MT1-MMP-mCh were treated as in A and time series were acquired by spinning-disk microscopy (see Video 2). Still images from the time series are shown. Arrows point to tubular extensions emanating from MT1-MMP–positive endosomes in cells depleted of WASH. Bars, 5 µm. (D) MDA-MB-231 cells treated with the indicated siRNA were processed for immunofluorescence microscopy with antibodies against cortactin (red) and WASH (green). Images were acquired by 3D deconvolution microscopy of the

WASH is present at docking sites of MT1-MMP–positive endosomes corresponding to invadopodia

Given that MT1-MMP is the key component for pericellular matrix degradation by invadopodia and that the exocyst complex is involved in MT1-MMP delivery to these structures (Sakurai-Yageta et al., 2008; Liu et al., 2009), we investigated whether WASH was also associated with invadopodia. Immunofluorescence microscopy of MDA-MB-231 cells plated on fluorescent gelatin revealed MT1-MMP–positive endosomes flanked by WASH-positive puncta in contact with the plasma membrane, some of which were associated with matrix degradation (Fig. 3, A–C). Observation by total interference reflection fluorescence microscope (TIRFM) of cells plated on a thin layer of cross-linked gelatin coexpressing MT1-MMPmCherry and GFP-tagged WASH or Exo84 showed that puncta of WASH and Exo84 associated with MT1-MMP–positive endosomes were in close contact with the adherent plasma membrane (Fig. 3, D and E). Similarly, WASH-positive puncta associated with MT1-MMP–containing endosomes were visible at the plasma membrane in BT-549 cells by TIRFM (Fig. 3 F). We also observed MT1-MMP–positive endosomes flanked by plasma membrane–apposed puncta containing Arp2/3, FAM21, cortactin, and Exo84 (Fig. 3, G and H; and Fig. S3, A and B). Matrix degradation was strictly confined to and superimposed upon WASH–FAM21–cortactin–Arp2/3–exocyst puncta adjacent to MT1-MMP–containing endosomes (Fig. 3, A, G, and H, arrowheads; and Fig. S3, A and B, arrowheads), strongly suggesting that these structures represent bona fide invadopodia. TIRFM of GFP-cortactin and MT1-MMPmCh documented repeated docking of MT1-MMP–containing endosomes at the level of cortactin-positive invadopodia (Fig. 3, I and J; and Video 3). Interestingly, although all invadopodia were positive for N-WASP, association of WASH with cortactin-positive invadopodia was inversely correlated with the surface of matrix degradation underlying each invadopodium (Fig. 3 K and Fig. S3 C). These results suggest that WASH, associated with MT1-MMP–positive endosomes, interacts transiently with invadopodia and preferentially at an early stage of their lifetime (associated with smaller degradation area) in contrast to N-WASP that is permanently associated with invadopodia.

Invadopodia correspond to late endosome-to-plasma membrane connections

Based on the proposed role of WASH-mediated Arp2/3 activation in the formation of endosomal tubular membrane extensions (Puthenveedu et al., 2010; Gomez et al., 2012; Piotrowski et al., 2013), we hypothesized that WASH puncta, possibly in conjunction with the exocyst complex, may regulate the formation of transient continuities between late endosomes and the invadopodial plasma membrane to allow the delivery of MT1-MMP for matrix degradation. We added a tracer to the extracellular milieu to test whether the endosome lumen was accessible through such connections. MDA-MB-231 cells expressing MT1-MMPmCh were plated on fluorescent gelatin and FITC-dextran was added for a 1-min pulse; then cells were examined immediately after washing out the tracer. A subset of MT1-MMP–positive endosomes were loaded with FITC-dextran during the pulse (Fig. 4 A, arrowheads), some exocytosed their MT1-MMP content while filling up with the dextran (Fig. 4 A, doublehead arrow). Cortactin-rich puncta and foci of matrix degradation were seen adjacent to FITC-dextran pulse-labeled endosomes (Fig. 4, B and C, arrowheads). In addition, after a 1-min pulse, fluorescent dextran–labeled endosomes were positive for Rab7 and VAMP7, arguing that these represent late endosomes making direct connection with the plasma membrane (Fig. 4, D and E). Furthermore, by live-cell TIRFM we observed regurgitation of the luminal FITC-dextran content of endosomes, some occurring through visible thin tubules extending from the endosome (Fig. 4 F). MT1-MMP–containing tubule emanating from plasma membrane–docked endosome was also visible by TIRFM (Fig. 4 G). These observations suggest the existence of tubular connections between MT1-MMP–positive late endosomes and the invadopodial plasma membrane that may mediate MT1-MMP delivery to the surface.

MT1-MMP exocytosis requires WASH and the exocyst complex

We used TIRFM to analyze the effect of silencing of WASH or Exo84 on the density of MT1-MMPmCh–positive endosomes in the zone beneath the plasma membrane. Large numbers of MT1-MMP vesicles were visible at the adherent plasma membrane of MDA-MB-231 cells (Fig. 5 A). Silencing of WASH or Exo84 significantly reduced MT1-MMP–positive endosome density beneath the plasma membrane (Fig. 5, A and B), along with the observed collapse of MT1-MMP–positive endosomes in the cell center (Fig. 2, A and C). All together, these findings indicate that both WASH and the exocyst complex play an important role in polarization and tethering of MT1-MMP–positive endosomes at the plasma membrane. The contribution of WASH and Exo84 to the delivery of MT1-MMP to the invadopodial plasma membrane was assessed by quantifying the surface accumulation of MT1-MMPpHluorin (Lizárraga et al., 2009); fluorescence of this construct is eclipsed in the acidic environment of the late endosome and rises upon exocytosis and exposure to the extracellular pH (Miesenböck, 2012). MT1-MMPpHluorin accumulated at the level of cortactin-positive invadopodia on the ventral cell surface (Fig. 5, C and D). Knockdown of WASH or Exo84 led to a 50% reduction of surface

middle plane of the cells. A region of interest (dashed line) was drawn manually around WASH-cortactin structures for quantification (shown in E). Bars, 5 µm. (E) Quantification of the integrated intensity of perinuclear endosomal cortactin and WASH in cells treated as in D and normalized to the integrated intensity in control cells in two independent experiments. ns, not significant; *, $P < 0.05$; **, $P < 0.01$ compared with control. (F) MDA-MB-231 cells treated with the indicated siRNAs were processed for immunofluorescence microscopy with cortactin and WASH antibodies and analyzed by high-resolution (~100-nm spatial resolution) 3D SIM. Bar, 1 µm. (G) Quantification of the projected surface of WASH and cortactin puncta in cells as described in F, normalized to mean projected surface of the puncta in control cells set to 100 (three independent experiments; $n = 25$ puncta for each condition; *, $P < 0.05$; ***, $P < 0.001$ compared with control).

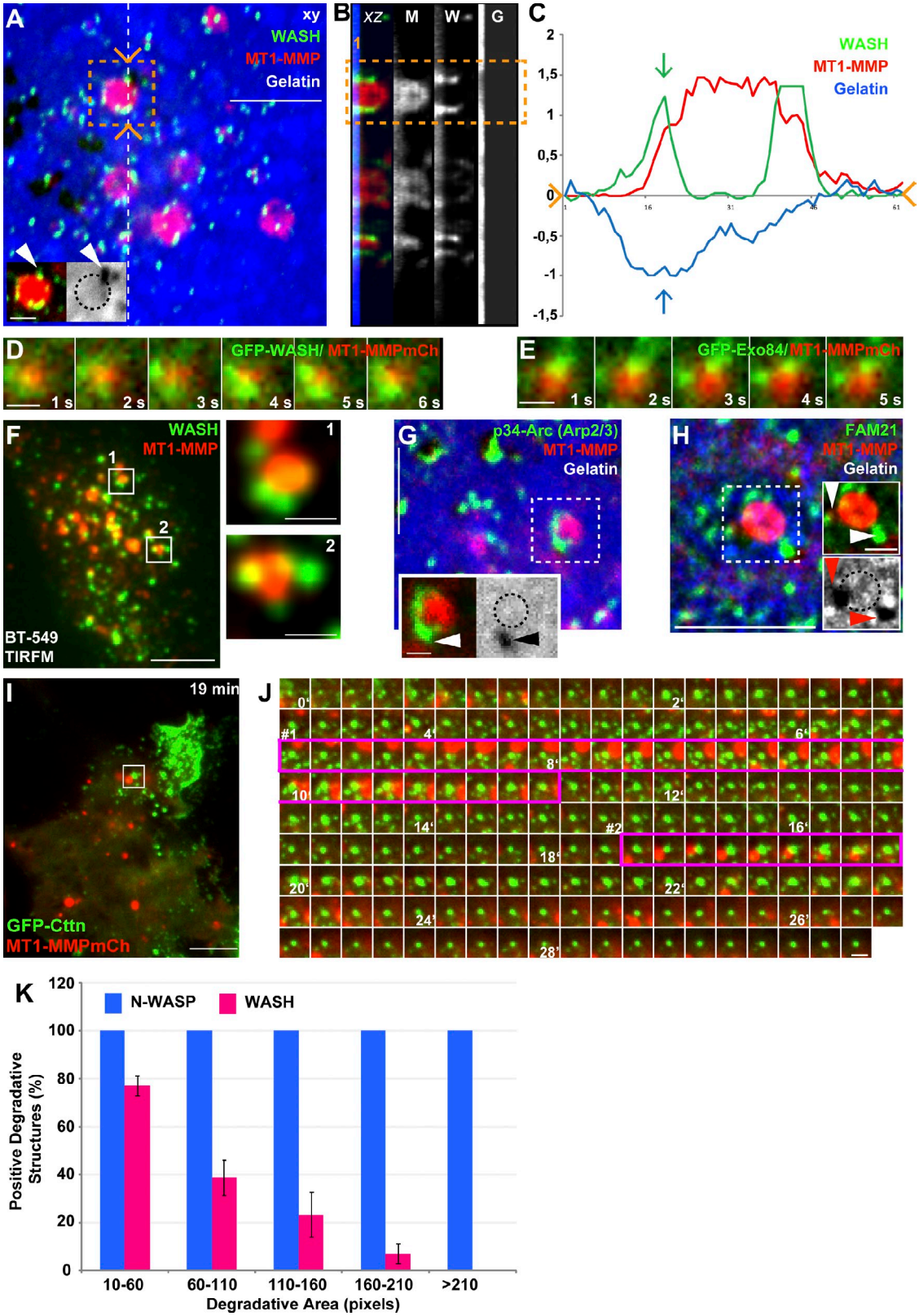

Figure 3. **Association of WASH endosomal puncta with invadopodia.** (A) MDA-MB-231 cells plated on cross-linked FITC-labeled gelatin (blue) were stained with antibodies against MT1-MMP (red) and WASH (green) and imaged by 3D deconvolution microscopy. Image is a single section in the ventral plane of the cell in contact with gelatin. Insets corresponding to the boxed region show split channels with dashed line representing the contour of the MT1-MMP–containing endosome projected on the FITC-gelatin image. Arrowhead points to matrix degradation restricted to WASH puncta adjacent to MT1-MMP–positive endosome. Bars: (main) 5 µm; (inset) 1 µm. (B) Orthogonal section through the dashed line in A. From left to right: merged image, MT1-MMP (M), WASH (W), and FITC-gelatin (G) signals. (C) Fluorescence intensity profile through the dashed line in the boxed region in A (x-axis, in pixels; y-axis, in arbitrary units). (D and E) MDA-MB-231 cells expressing MT1-MMPmCh and GFP-WASH (D) or GFP-Exo84 (E) plated on cross-linked gelatin and

accumulations of MT1-MMPpHluorin (Fig. 5 E), indicating that WASH and exocyst complex are critical for MT1-MMP exocytosis at invadopodia.

WASH and exocyst complex are required for invasive migration through type I collagen

Silencing of MT1-MMP is known to reduce drastically the ability of MDA-MB-231 cells to degrade a matrix of cross-linked gelatin as a basement membrane mimick (Artym et al., 2006; Sakurai-Yageta et al., 2008; Fig. 6 A). Silencing of WASH diminished the proportion of cells that were able to degrade gelatin and led to a 60–80% reduction in these cells' capacity to do so, similar to the effect of silencing various subunits of the exocyst complex, e.g., Sec6, Sec8, and Sec10 (Sakurai-Yageta et al., 2008) and Exo84 (Fig. 6 A). MT1-MMP levels were unaffected by the various siRNA treatments (Fig. S2 E). By comparison, silencing of N-WASP also led to 60% inhibition of matrix degradation, similar to the effect seen on WASH depletion (Fig. 6 A). Thus, both plasma membrane- and endosome-associated actin nucleation-promoting factors, N-WASP and WASH, are required for invadopodia activity in breast tumor cells. In addition, depletion of WASH or Exo84 led to a significant reduction in the ability of MDA-MB-231 cells to invade through a layer of Matrigel, similar to MT1-MMP knockdown (Fig. 6 B).

Degradation of cross-linked gelatin and Matrigel is representative of carcinoma cells remodeling and breaching the basement membrane. MT1-MMP is also required for dissemination of cancer cells within fibrous type I collagen (Fig. 6 C; Sabeh et al., 2004, 2009; Wolf et al., 2007), thus the question arose whether or not the WASH- and exocyst-dependent mechanism of exocytosis of MT1-MMP–containing late endosomes also operated during remodeling of collagen fibers and invasive migration by tumor cells. We analyzed the capacity of MDA-MB-231 cells to invade the collagen I–filled, cell-free central portion of a 96-well plate over a 2-d culture period. Knockdown of WASH or Exo84 resulted in a strong inhibition of the invasion capacity of the cells in type I collagen similar to the silencing of MT1-MMP (Fig. 6, C and D). In addition, we found that silencing of WASH or Exo84 resulted in a 75–85% inhibition of pericellular collagen I degradation revealed by the Col1-$^{3/4}$C antibody recognizing the cleaved fragment of collagen I dependent on MT1-MMP activity as indicated by the reduction of Col1-$^{3/4}$C signal on MT1-MMP depletion (Fig. 6, E and F; Wolf et al., 2007). Thus these data indicate a general requirement for the exocyst complex and WASH for matrix remodeling and for the invasive potential of breast tumor cells.

Exocytosis of MT1-MMP occurs at contact sites with type I collagen fibers through a WASH- and exocyst-dependent mechanism

We analyzed the organization and dynamics of invadopodia in cells invading through 3D type I collagen environments in relation with WASH- and exocyst-positive MT1-MMP–containing endosomes. Staining of the cells for F-actin and cleaved collagen I fibers (Col1-$^{3/4}$C antibody) revealed the formation of linear accumulations of F-actin on the inner face of the plasma membrane associated with collagen fibers, coincident with regions of collagenolytic activity (Fig. 7 A). These structures have been previously reported and named linear invadopodia (Juin et al., 2012). Similarly to classical dotty-like invadopodia on gelatin (Fig. S3 C), N-WASP colocalized with F-actin in linear invadopodia (Fig. 7 B). Labeling with anti-WASH antibodies showed the typical pattern of endosomal WASH-positive puncta (Fig. 7 C), some of which were closely apposed to linear invadopodia stained for cortactin although WASH did not accumulate in linear invadopodia (Fig. 7, C [inset], D, and E). We used live-cell imaging to analyze the dynamic interactions of WASH- and cortactin-positive puncta with linear invadopodia in cells in a 3D fibrillar collagen environment. Live-cell imaging of MDA-MB-231 cells expressing DsRed-cortactin and GFP-WASH (Video 4 and Fig. 7, D and E) plated on a layer of fluorescent collagen I fibers revealed the dynamic assembly of cortactin-positive linear invadopodia along collagen fibers and their disassembly upon remodeling and relaxation of the underlying fibers (Video 4 and Fig. 7 E). In addition, cortactin- and WASH-positive endosomal puncta interacted highly dynamically with linear invadopodia (Video 4 and Fig. 7, D and E). On examination of the time-lapse sequences there was no obvious transfer of cortactin from endosomal puncta to the linear invadopodia (Fig. 7 E). Analysis of MT1-MMP distribution in fixed cells showed that cortactin puncta were associated with MT1-MMP–positive endosomes (Fig. 7, F and G, arrows) in the vicinity of linear invadopodia positive for cortactin and MT1-MMP (Fig. 7, G and H, arrowheads), in agreement with the collagenolytic activity of these structures. All together, these data suggested that collagen I fibers elicit actin assembly and the formation of N-WASP–positive collagenolytic linear invadopodia and the dynamic recruitment of WASH-cortactin–positive endosomes probably involved in MT1-MMP delivery to these structures.

Exocytic events of MT1-MMP were monitored in live cells cultured on fibrillar collagen using the MT1-MMPpHluorin construct. In cells expressing simultaneously mCherry- and pHluorin-tagged MT1-MMP, dynamic late endosomes (red) were observed in the cytoplasm, with visible green flashes corresponding

analyzed by live-cell dual color TIRFM. Time interval between each image is 1 s. Bars, 1 µm. (F) BT-549 cells plated on cross-linked gelatin were fixed and immunostained for MT1-MMP and WASH and analyzed by TIRFM. Insets are higher magnification views of the boxed regions. (G and H) Cells treated as in A, stained with antibodies against MT1-MMP (red) and p34-Arc subunit of Arp2/3 complex (G, green) or FAM21 (H, green). Arrowheads point to the accumulation of the markers near degradative invadopodia adjacent to MT1-MMP–positive endosomes. Bars: (main) 5 µm; (inset) 1 µm. (I) MDA-MB-231 cells expressing GFP-cortactin and MT1-MMP-mCh plated on cross-linked gelatin and analyzed by dual color TIRFM. A still image from a representative time-lapse series is shown. (J) A series of time-lapse TIRFM images corresponding to the boxed region in panel I. Numbers in the series of time-lapse images represent the time in minutes. Two events of docking of MT1-MMP–containing endosomes (labeled #1 and #2) are boxed in pink. (K) Cells as in A were stained for cortactin and WASH or N-WASP. The graph shows the percentage of WASH- (pink bars) or N-WASP–positive (blue bars) degradative invadopodia positive for cortactin (not depicted) as a function of the surface of matrix degradation (in pixels). Values are means ± SEM scoring 360 invadopodia from 15 WASH-labeled cells and 135 invadopodia from five N-WASP–labeled cells.

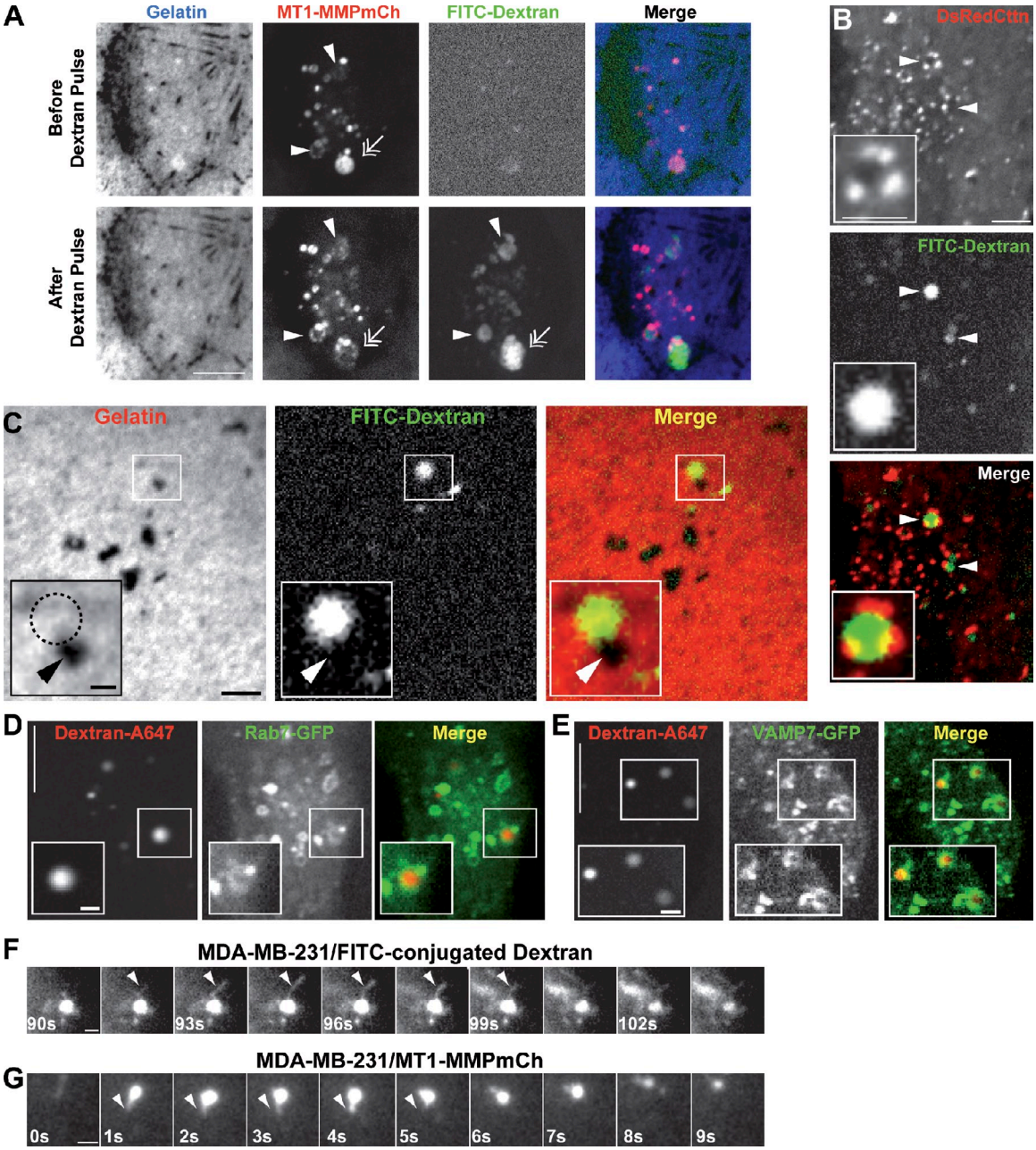

Figure 4. **Tubular connection between MT1-MMP–containing late endosomes and the invadopodial plasma membrane.** (A) MDA-MB-231 cells expressing MT1-MMPmCh were plated on cross-linked gelatin. One optical section was taken in the ventral plane of the cells by confocal spinning disk microscopy (top). A second optical section was taken after a 1-min pulse of FITC-dextran added to the medium (bottom). Arrowheads point to MT1-MMP–positive endosomes filled with FITC-dextran during the pulse. The double-headed arrow points to an endosome that lost its MT1-MMP content and filled up with FITC-dextran. Bar, 5 µm. (B) MDA-MB-231 cells expressing DsRed-cortactin treated as in A and imaged immediately after the FITC-dextran pulse. Arrowheads point to cortactin-positive puncta adjacent to dextran-labeled endosomes. Bars, 5 µm. (C) MDA-MB-231 cells expressing MT1-MMPmCh (not depicted) were plated on cross-linked fluorescent gelatin, pulsed with FITC-dextran, and analyzed by confocal spinning disk microscopy 1–2 min after the pulse. Arrowheads point to focal degradation of the matrix adjacent to a FITC-labeled endosome. Dashed line represents the contour of the FITC-dextran–containing endosome projected on the gelatin image. (D and E) MDA-MB-231 cells expressing Rab7-GFP (D) or VAMP7-GFP (E) were plated on cross-linked gelatin for 5 h. An optical section was taken immediately after a 1-min pulse of A647-dextran added to the medium. Insets are higher magnification views of the boxed regions that point to Rab7- (D) or VAMP7 (E)-positive endosomes filled with A647-dextran during the pulse. Bars: (main) 5 µm; (insets) 1 µm). (F) Live-cell imaging of MDA-MB-231 cells analyzed by TIRFM immediately after the FITC-dextran pulse. The indicated times in the image gallery are seconds after the pulse. Arrowhead points to a tubular extension emanating from the FITC-dextran–labeled endosome during regurgitation of the fluid-phase tracer. Bar, 2 µm. (G) MDA-MB-231 cells expressing MT1-MMPmCh analyzed by TIRFM. The arrowhead points to an MT1-MMP–positive tubule. Bar, 1 µm.

to the de-quenching of pHluorin fluorescence upon exocytosis (Video 5 and Fig. S4). Endosomes scanning portions of the plasma membrane in contact with collagen I fibers were visible (Video 5 and Fig. S4, A and B, $t = 0$ min), which underwent repeated exocytosis in the vicinity of the collagen fibers (Fig. S4, A and B, arrowheads). Live-cell imaging of cells expressing MT1-MMPpHluorin and mCherry-WASH showed that MT1-MMP–containing endosomes undergoing exocytosis were

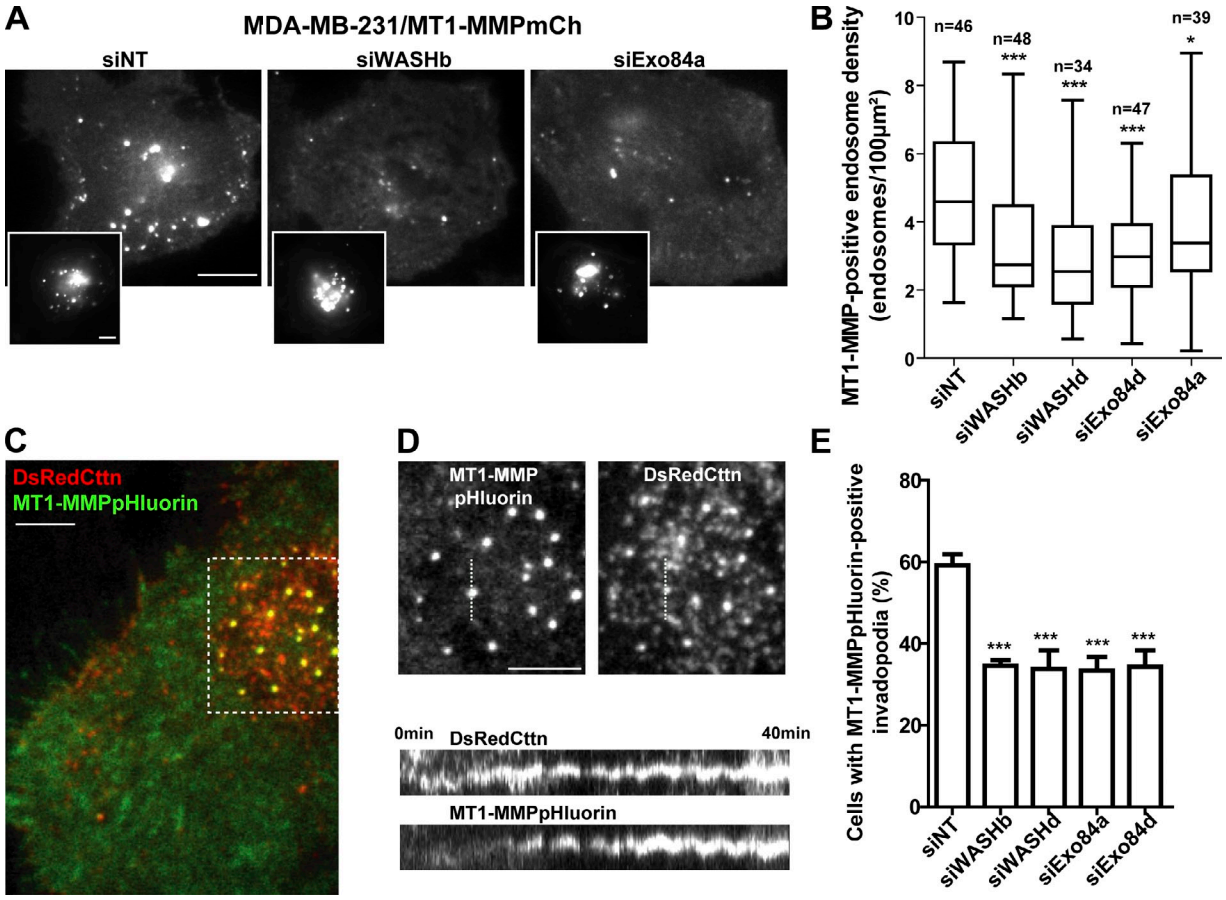

Figure 5. **WASH and exocyst complex are required for invadopodial degradation of the matrix.** (A) Effect of WASH or Exo84 silencing on the density of MT1-MMPmCh–positive vesicles in the subplasma membrane region of MDA-MB-231 cells observed by TIRFM. Insets are the corresponding wide-field images showing similar MT1-MMP expression. Bars, 5 µm. (B) Box plots showing the density of subplasma membrane MT1-MMP vesicles. Number of cells analyzed from four experiments is indicated (*n*). *, $P < 0.05$; ***, $P < 0.001$ (compared with control cells treated with siNT). (C) MDA-MB-231 cells expressing MT1-MMPpHluorin and DsRed-cortactin were plated on cross-linked gelatin for 2–3 h and analyzed by dual color TIRFM. A merged image from a representative time-lapse series is shown. (D, top) Split signals from the boxed region in C showing accumulations of MT1-MMPpHluorin at cortactin-positive invadopodia. Bar, 5 µm. (bottom) Kymograph views of TIRF time series acquired every 10 s. (E) MDA-MB-231 cells expressing MT1-MMPpHluorin were treated with the indicated siRNAs, plated on cross-linked gelatin, and analyzed by TIRFM. Plots show the percentage of cells with MT1-MMPpHluorin–positive invadopodia. Values are means ± SEM from three independent experiments scoring a total of 150–200 cells for each cell population. ***, $P < 0.001$ (compared with cells treated with non-targeting siRNA).

flanked by WASH puncta (Video 6 and Fig. 8, A and B, red arrowheads) and exocytosis preferentially occurred at contact sites with fibers (Video 6 and Fig. 8, A and B, green arrowheads). Multiple exocytic events led to surface accumulation of MT1-MMP along the collagen fibers (at linear invadopodia; Fig. 8 A, white arrowheads) and fiber remodeling (Video 6). Quantitative assessment of MT1-MMPpHluorin flashes revealed a strong inhibition of MT1-MMP exocytic events upon knockdown of WASH or Exo84 (Fig. 8 C), whereas overall MT1-MMP expression was similar in the different cell populations (not depicted).

So far, our observations were compatible with a WASH/Exocyst-dependent mechanism whereby MT1-MMP–positive endosomes exocytose the protease at contact sites with collagen fibers but do not collapse within the plasma membrane bilayer. They also revealed that MT1-MMPpHLuorin flashes lasted for several minutes (Fig. 8 D). In addition, we noticed that although some endosomes with de-quenched MT1-MMPpHluorin were moving along fibers and could possibly detached and reengage with other sites for multiple rounds of MT1-MMP exocytosis, some remained at the same position for several minutes (Videos 5 and 6; Fig. S4; and Fig. 8, A and B). These findings raised the issue of the duration of endosome-to-plasma membrane openings. Using an extracellular pH shifts protocol (Video 7; Perrais et al., 2004), we observed that some endosomes remained opened for several minutes as shown by the fluorescence of pHluorin in the endosomal lumen that was sensitive to the iterative shifts of extracellular pH (at least for 4 min in the example shown in Fig. 8 E and up to 15 min [not depicted]). Of note, similar long-lasting fusion pore openings have been reported during zymogen granule exocytosis in exocrine pancreatic acinar cells (up to 15 min; Perrais et al., 2004; Thorn et al., 2004; Sokac and Bement, 2006). Moreover, the exchange of low and high pH solution within the endosome could take up to 30 s, consistent with the restricted diffusion of solutions through a long tubular connection. Thus, through the functions of WASH and exocyst complex, tumor cells can engage late endocytic MT1-MMP storage compartment in the formation of tubular continuities with the

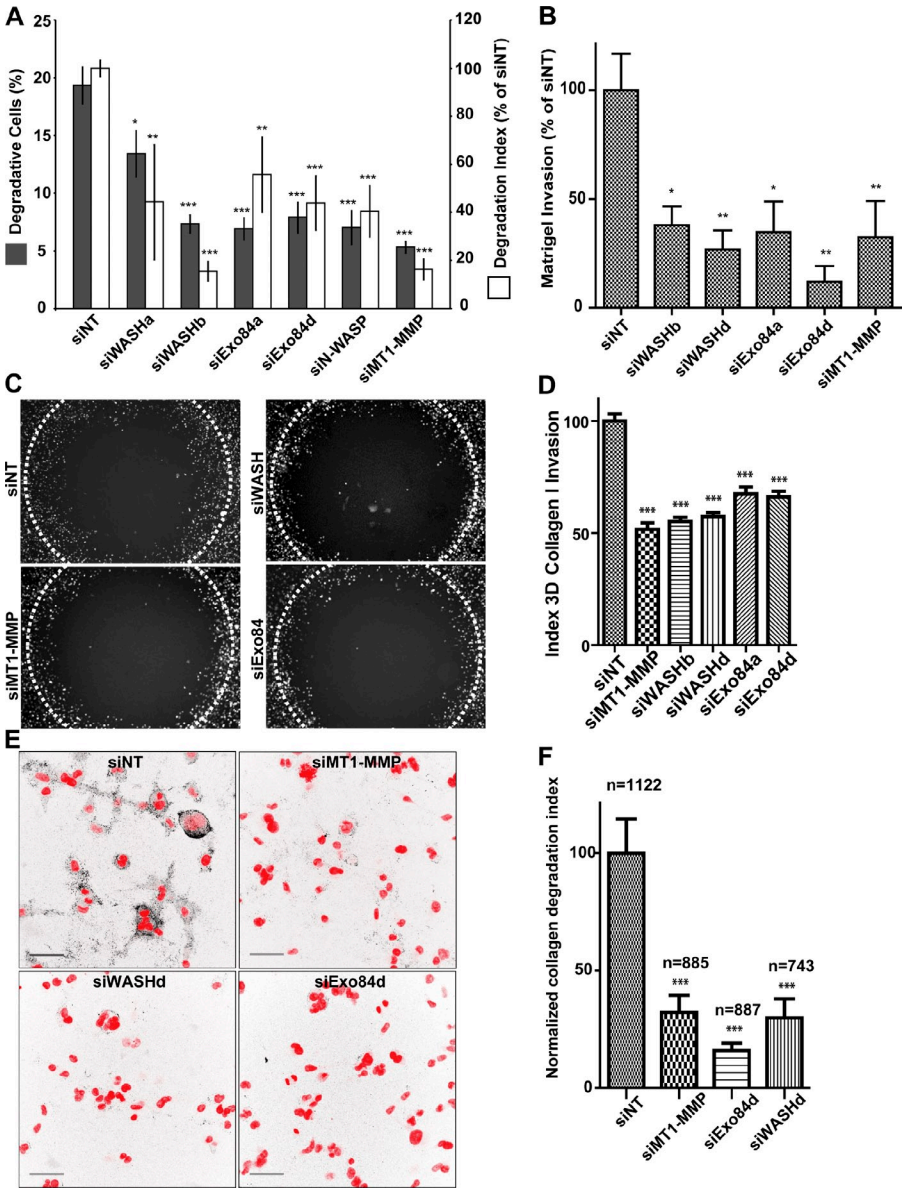

Figure 6. **WASH and exocyst complex are required for matrix remodeling and the invasive potential of breast tumor cells.** (A) MDA-MB-231 cells treated with indicated siRNAs were plated on cross-linked FITC-labeled gelatin and the percentage of degradative cells (gray bars) and the degradation index (white bars) were calculated. Values are means ± SEM from at least three independent experiments scoring a total of 300–400 cells for each siRNA. *, $P < 0.05$; **, $P < 0.01$; ***, $P < 0.001$ (compared with siNT-treated cells). (B) MDA-MB-231 cells treated with indicated siRNAs were quantified on the lower side of the Transwell filter after invasion through Matrigel. Values are mean ± SEM of normalized percentage from two to three independent experiments. *, $P < 0.05$; **, $P < 0.01$ (compared with siNT-treated cells). (C) 3D type I collagen circular invasion assay of MDA-MB-231 cells expressing Histone-2B-GFP treated with indicated siRNAs after 48 h. Dashed circles represent the collagen–cell interface at time 0. (D) Values represent mean invasion index ± SEM for the different cell populations from three independent experiments, normalized to cells treated with non-targeting siRNA (***, $P < 0.001$). (E) MDA-MB-231 cells treated with the indicated siRNAs were embedded in collagen I. Pericellular collagenolysis was detected using anti-Col1-$^{3/4}$C antibodies (in black in the inverted image). Nuclei were stained with DAPI (red). Bars, 50 µm. (F) Quantification of collagenolysis by MDA-MB-231 cells treated with the indicated siRNAs. Values are mean normalized degradation index ± SEM from three (siNT, siExo84d, and siMT1-MMP) or two independent experiments (siWASHd). *n* represents the number of cells analyzed for each cell population. ***, $P < 0.001$ (as compared with siNT-treated cells).

plasma membrane at contact sites with the extracellular matrix to allow delivery of the protease to the surface and to ensure matrix remodeling required for invasive migration.

Discussion

Our data, which are summarized in a model presented in Fig. 9, support a general mechanism of invadopodia formation whereby the functions of WASH and exocyst complex on closely apposed punctate domains on the cytosolic face of MT1-MMP–positive late endosomes ensure focal delivery of MT1-MMP for pericellular matrix degradation.

We found that loss of WASH function induces disappearance of endosomal F-actin puncta and a collapse of MT1-MMP–positive late endosomal system, which is accompanied by defects in MT1-MMP recycling and delivery to the invadopodial plasma membrane. This is in agreement with an established function of the WASH complex in the recycling route of various plasma membrane proteins in different cell types (Derivery et al., 2009; Gomez and Billadeau, 2009; Zech et al., 2011; Gomez et al., 2012; Piotrowski et al., 2013). In addition, the exocyst complex, which mediates the tethering of exocytic vesicles to the plasma membrane, is also required for the delivery of MT1-MMP to invadopodia (Sakurai-Yageta et al., 2008; Liu et al., 2009; this study). Strikingly, our study reveals that WASH- and F-actin–positive puncta on MT1-MMP endosomes are adjacent to exocyst-positive puncta on this compartment and some components of these two multiprotein complexes (WASH, Exo84, and Sec3 based on two-hybrid data) can interact with each others. The segregation of WASH domains on the cytolic face of the endosomal membrane depends on actin polymerization, which is induced by WASH-mediated activation of the Arp2/3 complex (Derivery et al., 2012). The mechanism underlying the subdomain organization of the exocyst complex at the surface of MT1-MMP–positive endosomes is presently unknown; however, we found that exocyst components can negatively regulate WASH-dependent endosomal actin

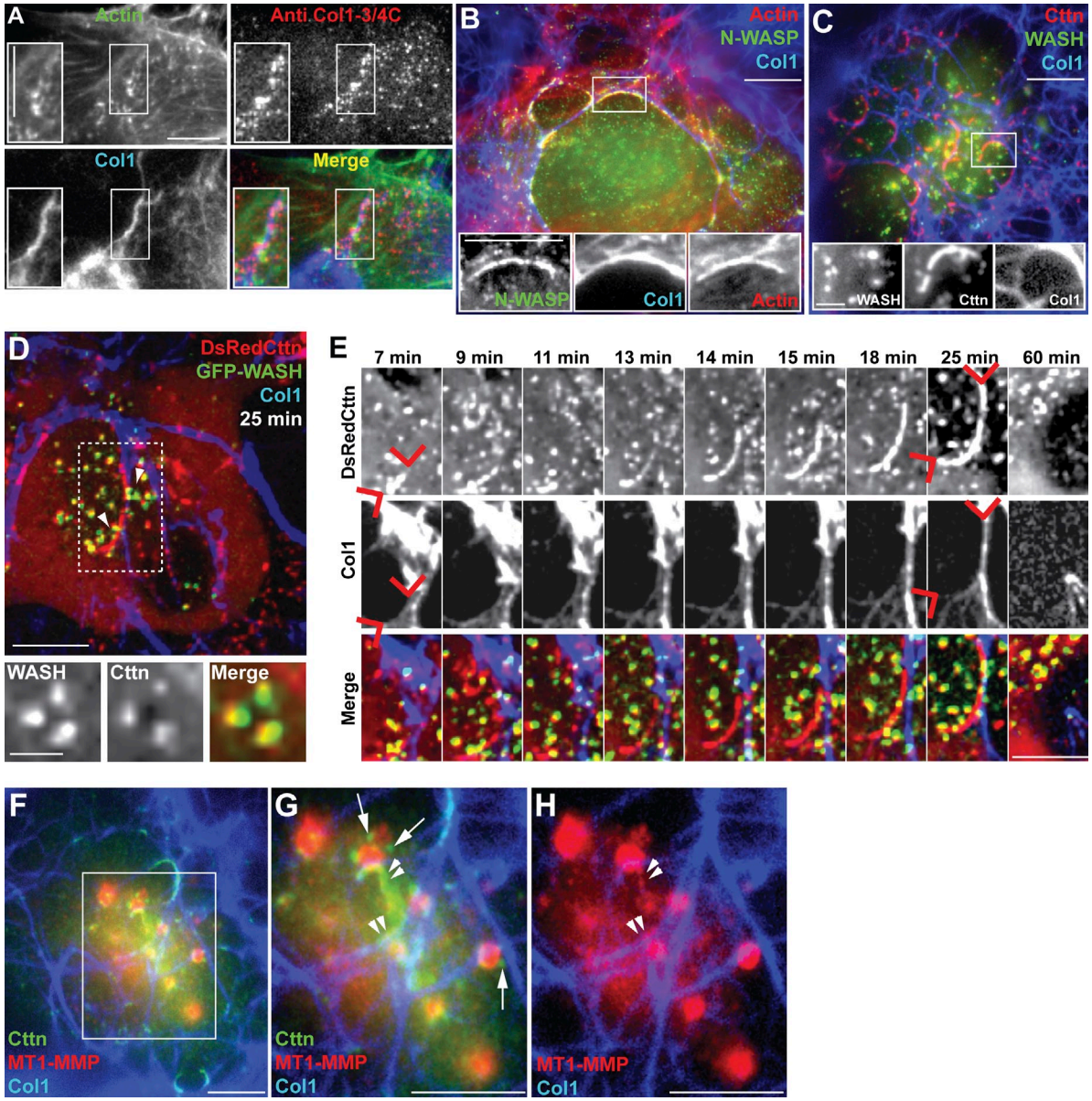

Figure 7. **WASH- and cortactin-positive MT1-MMP–containing endosomes are recruited in the periphery of linear invadopodia in association with collagen fibers.** (A) MDA-MB-231 cells on a layer of collagen I fibers stained with anti-Col1-$^{3/4}$C antibodies recognizing MMP-cleaved collagen I (red) and for F-actin (green) revealing collagenolytic linear invadopodia. Inset is a higher magnification of the boxed region. Bars, 5 µm. (B and C) Cells were plated on a layer of Alexa Fluor 647–conjugated type I collagen (blue) for 30 min and stained for N-WASP (green) and F-actin (red; B) or WASH (green) and cortactin (red; C). Insets are higher magnification of boxed regions. Bars: (main and B [inset]) 5 µm; (C, inset) 1 µm. (D) MDA-MB-231 cells expressing GFP-WASH (green) and DsRed-cortactin (red) were plated on a layer of Alexa Fluor 647–conjugated type I collagen (blue) for 30 min and imaged by confocal spinning disk microscopy. A still image from a representative time-lapse series is shown (t = 25 min). Arrowheads point to WASH- and cortactin-positive puncta (associated with late endosomes) apposed to a cortactin-positive linear invadopodium aligned on collagen fibers. Insets show a higher magnification of WASH and cortactin endosomal puncta. The corresponding time-lapse series is shown in Video 4. Bars: (main) 5 µm; (inset) 1 µm. (E) Higher magnification of the boxed region in D at representative time points. A linear cortactin-positive invadopodium aligned with collagen fibers forms on the inner face of the plasma membrane (13–14 min; red arrowheads); at 60 min, this structure disassembled while collagen I fibers were remodeled. Time is in minutes. Bar, 5 µm. (F–H) Cells on Alexa Fluor 647–conjugated type I collagen (blue) stained for MT1-MMP (red) and cortactin (green). G and H are higher magnification of the boxed region in F. Arrows point to cortactin-positive puncta associated with MT1-MMP–containing endosomes in the vicinity of cortactin- and MT1-MMP–positive linear invadopodia (arrowheads). Bars, 5 µm.

assembly. In this respect, two-hybrid data mapping of the binding site of Exo84 and Sec3 exocyst subunits to the amino-terminal region of WASH suggests a possible competition mechanism because this region of WASH is also required for association with other WASH complex components (Gomez and Billadeau, 2009; Jia et al., 2010). A consequence of exocyst's interaction with WASH could thus be a fine regulation of actin assembly required for late endosome organization and for MT1-MMP recycling to the surface. Therefore, in addition to its well-established function as a tethering factor for exocytic vesicles to the plasma membrane (Heider and Munson, 2012), our findings suggest an unprecedented role for the exocyst in regulating endosomal membrane dynamics.

Remarkably, we found that MT1-MMP–positive endosomes contact and establish connections with the plasma membrane in

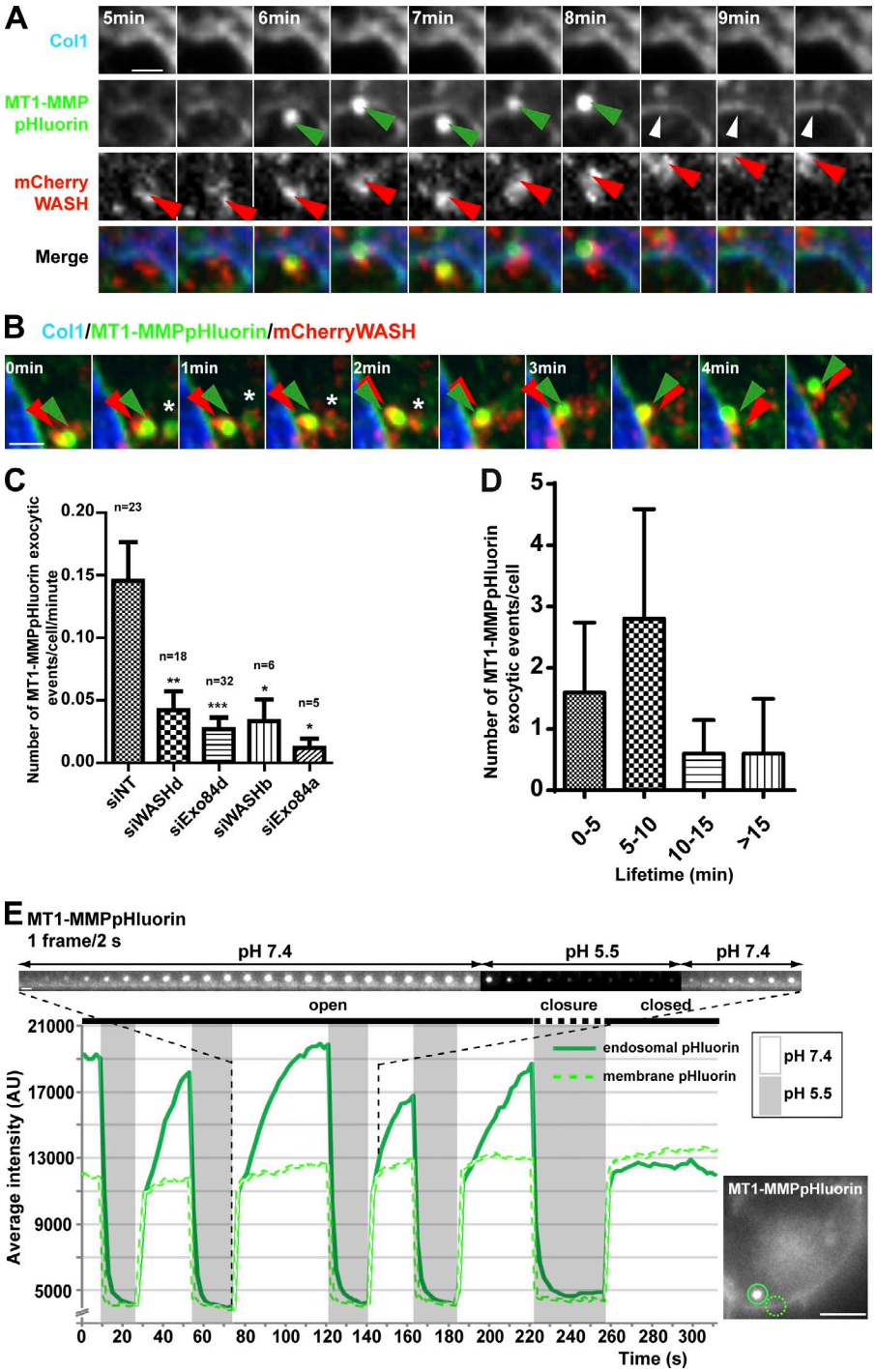

Figure 8. **A WASH- and Exo84-dependent exocytic mechanism of MT1-MMP involved in pericellular collagenolysis.** (A and B) Live-cell imaging of MDA-MB-231 cells expressing MT1-MMPpHluorin (green) and mCherry-WASH (red) constructs, plated on a layer of collagen I for 30 min (see Video 6). The galleries show exocytosis of MT1-MMPpHluorin–positive endosomes (green arrowheads) in the vicinity of a collagen type I fiber (blue). These endosomes harbor WASH-positive patches (red arrowheads). The asterisks in B point the reacidification of a WASH- and MT1-MMPpHluorin–positive endosome. Time is represented in minutes. Bars, 2 µm. (C) MDA-MB-231 cells expressing MT1-MMPmCherry and MT1-MMPpHluorin silenced for the indicated proteins were seeded on a layer of type I collagen fibers and imaged over a 30-min time perios and the frequency of MT1-MMPpHLuorin exocytic events was quantified (box plots of events/cell/min). The number of cells analyzed for each cell population is indicated. *, $P < 0.05$; **, $P < 0.01$; ***, $P < 0.001$ (compared with siNT-treated cells). (D) Lifetime of MT1-MMPpHluorin–positive flashes (in minutes). Data show the number of pHLuorin exocytic flashes per cell for the different lifetimes ± SEM from five cells out of three independent experiments. (E) MDA-MB-231 cells expressing MT1-MMPpHluorin were cultured on a layer of Cy3-labeled type I collagen fibers and subjected to external pH shifts alternating between 7.4 (white zones) and 5.5 (gray zones). The plots represent pHLuorin intensity of a MT1-MMP–positive endosome that underwent exocytosis (circled with a solid line in the inset on the right) and of a region of the plasma membrane (dashed line). The corresponding time-lapse series is shown in Video 7. The gallery above the plot represents a sequence starting with external pH 7.4 corresponding to the circled MT1-MMPpHLuorin–positive endosome (see inset). Bars: (inset) 5 µm; (gallery) 1 µm.

contact with the matrix (basement membrane or fibrous type I collagen) at the level of WASH–F-actin–cortactin– and exocyst-positive puncta. These connections, most likely tubular, that form between late endosomes and the plasma membrane allow exocytosis of MT1-MMP to the surface and they occur at and correspond to bona fide invadopodia. It is currently though that WASH-dependent actin assembly can generate the force to drive the formation of endosomal tubular extensions (Puthenveedu et al., 2010; Derivery et al., 2012; Gomez et al., 2012; Piotrowski et al., 2013). This, together with the capacity of the exocyst complex to mediate membrane tethering and modulate WASH-dependent actin assembly (He and Guo, 2009; Hertzog and Chavrier, 2011; this study), suggests a mechanism whereby WASH and exocyst may work in a coordinated manner to control the formation of endosome-to-plasma membrane connections ensuring MT1-MMP targetting to the invadopodial plasma membrane. In addition, the exocyst complex is known to control SNARE complex assembly and to influence vesicle fusion (Heider and Munson, 2012). Thus, the exocyst could regulate membrane fusion at invadopodial endosome-to-plasma membrane connections. Whether the exocyst can interact and influence the activity of the late endosome SNARE protein VAMP7, which is required for MT1-MMP

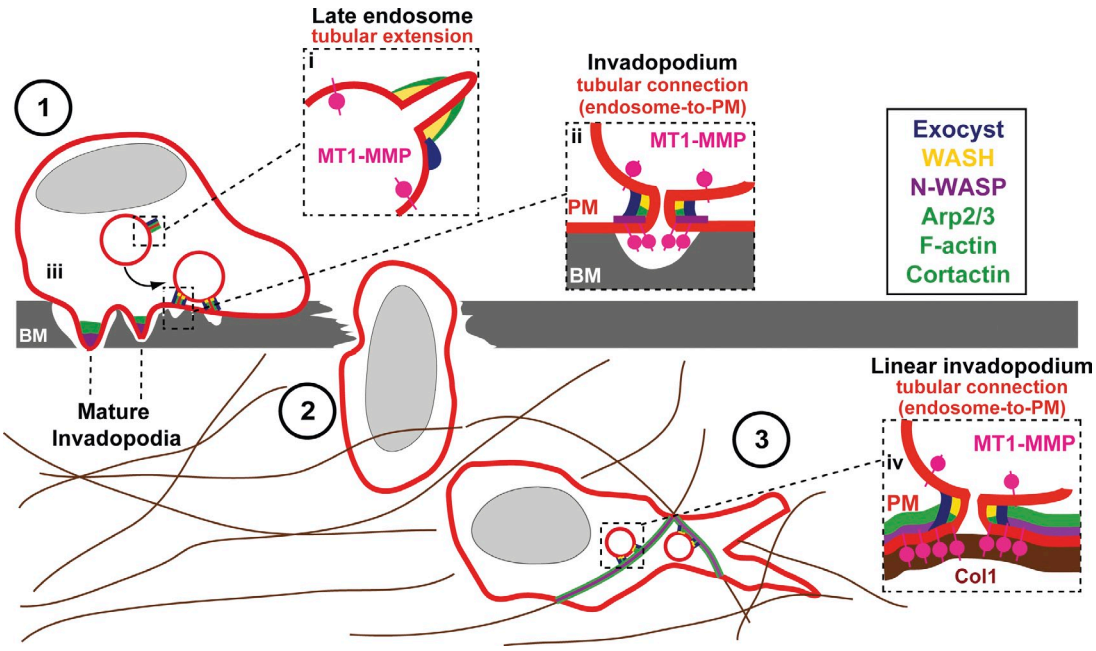

Figure 9. **Schematic model of the general mechanism of exocytosis of MT1-MMP–positive late endosomes at the invadopodial plasma membrane.** WASH-dependent Arp2/3 complex activation and actin/cortactin assembly controls the dynamics of tubular endosomal membrane extensions (inset i) and tubular endosome-to-plasma connections required for transfer and delivery of MT1-MMP from the endosome to the invadopodial plasma membrane (inset ii). The exocyst complex mediates tethering of MT1-MMP–positive late endosomes with the target membrane (ii). Fusion between the endosomal membrane tubule and the invadopodial plasma membrane may necessitate the SNARE protein VAMP7 (not depicted; Steffen et al., 2008; Williams and Coppolino, 2011). Actin and cortactin assembly at invadopodia requires N-WASP and allows membrane protrusion formation and retention of MT1-MMP (insets ii and iii; Yamaguchi et al., 2005; Artym et al., 2006; Oser et al., 2010; Yu et al., 2012). Mature invadopodia are responsible for penetrating and breaching the basement membrane in contact with carcinoma cells (1 and 2; Hotary et al., 2006; Rowe and Weiss, 2008). In the fibrous, collagen-rich extracellular membrane environment surrounding the tumor (3), fibers that oppose cell movement, involving recognition by yet unidentified collagen receptors, trigger the assembly of N-WASP– and F-actin–positive linear invadopodia and the recruitment and exocytosis of MT1-MMP–containing endosomes based on the conserved WASH and exocyst-dependent mechanism (inset iv).

delivery to invadopodia, has to be established (Steffen et al., 2008; Williams and Coppolino, 2011).

Our findings also demonstrate that exocytosis of MT1-MMP does not occur through complete collapse of MT1-MMP–positive endosomes into the plasma membrane, but by a mechanism whereby late endosomes are retrieved apparently intact after fission of endosome-to-plasma membrane connections and can possibly engage in multiple exocytic events. Strikingly, some of these connections remain open for several minutes; however, transfer of MT1-MMP from the storage endosome to the invadopodial plasma membrane is tightly controlled as a large portion of the protease remains associated with the endosome. Thus, the tubular connection forming between the two membrane compartments in a WASH/exocyst-dependent manner may exert different functions; it could stabilize and restrict the extension of the fusion pore between the two membranes and it may also act as a filter to prevent free diffusion of MT1-MMP out of the endosome. Along this line, it was recently shown that N-WASP–dependent invadopodial F-actin can prevent the diffusion of MT1-MMP out of the invadopodia through some interaction of the cytoplasmic domain of the protease with the actin network (Yu et al., 2012). The same type of interactions with WASH-dependent F-actin surrounding the connecting tube would limit diffusion of MT1-MMP out of the endosome and ensure controlled delivery of MT1-MMP to the plasma membrane for controlled remodeling of the basement membrane and collagen fibers.

Finally, this study supports the conclusion that two pools of F-actin–cortactin coexist and cooperate to ensure invadopodia formation and function. One pool is associated with and depends on N-WASP activity, which is associated with the core invadopodia structure forming on the cytoplasmic face of the plasma membrane in association with the matrix. These N-WASP–F-actin–cortactin–positive structures include typical dotty-like invadopodia forming on the adherent plasma membrane in cells on gelatin or basement membrane (Yamaguchi et al., 2005; Artym et al., 2006; Oser et al., 2010; Yu et al., 2012) and linear F-actin–based structures assembling in association with collagen fibers in tumor cells invading through a 3D fibrous environment (Juin et al., 2012; Yu et al., 2012; this study). These different structures represent docking sites for MT1-MMP–containing endosomes and may provide a physical scaffold for plasma membrane protrusion and MT1-MMP retension to penetrate the extracellular matrix and basement membrane. The second pool, with a punctate organization, is associated with and depends on WASH activity on MT1-MMP–positive endosomes and, together with other components including the exocyst complex, contributes to an exocytic mechanism that fuels the invadopodia with the proteolytic activity necessary for pericellular matrix remodelling. The coordinated function of WASH and the exocyst complex in the fundamental biology of invadopodium-mediated proteolysis in different pathologically relevant matrix environments demonstrated here appears a crucial part of the invasive program of carcinoma cells.

Materials and methods

Antibodies and constructs

Antibodies used in this study are listed in Table S1. Full-length mouse WASH cDNA amino-terminally fused with GFP or mCherry was subcloned in pcDNA3.1 vector (Derivery et al., 2009). Full-length rat cortactin cDNA (provided by M.A. McNiven, Mayo Clinic, Rochester, MI) was subcloned in pDsRed1-N1 and pEGFP-N1 (Takara Bio Inc.) in fusion with carboxy-terminal DsRed or GFP, respectively. Human full-length Exo84 and Sec3 were subcloned in pcDNA3.1 plasmid with amino-terminal GFP or carboxy-terminal HA tags.

Yeast two-hybrid screening

The coding sequence for full-length human Sec3 (GenBank accession no. gi:7023219) and Exo84 (GenBank accession no. gi:58331103) were PCR amplified and cloned into pB27 as carboxy-terminal fusions to LexA. The constructs were checked by sequencing the entire inserts and used as baits to screen at saturation a highly complex human placenta domain library constructed into pP6. pB27 and pP6 derive from the original pBTM116 (Vojtek and Hollenberg, 1995) and pGADGH (Bartel et al., 1993) plasmids, respectively. For Sec3, 96 million clones (10-fold the complexity of the library) were screened using a mating approach with Y187 (matα) and L40ΔGal4 (mata) yeast strains as previously described (Fromont-Racine et al., 1997). 353 His^+ colonies were selected on a medium lacking tryptophan, leucine, and histidine, supplemented with 2 mM 3-aminotriazole. For Exo84, 64 million clones were screened and 164 His^+ colonies were selected using the same protocol. The prey fragments of the positive clones were amplified by PCR and sequenced at their 5′ and 3′ junctions. The resulting sequences were used to identify the corresponding interacting proteins in GenBank using a fully automated procedure. The protein interactions from this publication have been submitted to the IMEx consortium through IntAct (Kerrien et al., 2012) and assigned the identifier IM-17363.

Cell culture, DNA transfection, stable cell lines, and RNAi

The human breast adenocarcinoma cell line MDA-MB-231 (HTB-26; American Type Culture Collection) was maintained in L-15 culture medium (Sigma-Aldrich) with 2 mM glutamine and 15% FCS at 37°C in 1% CO_2. MDA-MB-231 cells stably expressing MT1-MMPmCherry (MT1-MMPmCh) were cultured in the same medium supplemented with 0.5 mg/ml G418 (Sakurai-Yageta et al., 2008). MDA-MB-231 cells stably expressing MT1-MMPpHluorin (Lizárraga et al., 2009), with the GFP-derivative pHluorin tag (super-ecliptic variant [Miesenböck, 2012]) inserted in the extracellular domain, were generated by lentiviral transduction. For transient expression, MDA-MB-231 cells were transfected with plasmid constructs (1 µg) using Lipofectamine LTX (Invitrogen) or Nucleofector (Lonza) according to the manufacturers' instructions. Cells were analyzed 48 h after transfection. BT-549 (HTB-122; American Type Culture Collection) human breast cancer cells were cultured in RPMI medium with 2 mM glutamine and 10% FCS at 37°C in 5% CO_2. siRNA transfection was performed using 50 nM siRNA with Lullaby reagent (OZ Biosciences). Cells were analyzed 72 h after treatment. The siRNA sequences used in this study are shown in Table S2.

Immunoprecipitation

For expression of HA-tagged Exo84 and Sec3 exocyst complex subunits, HeLa cells were transiently transfected using FuGENE (Roche) according to the manufacturer's instructions. 48 h after transfection, cells were lysed in lysis buffer (50 mM Tris-HCl, pH 7.4, 150 mM NaCl, 1% Triton X-100, 1 mM EDTA, and complete Mini Protease Inhibitor Cocktail; Roche), and then centrifuged at 13,000 rpm for 10 min at 4°C. Supernatants (1–2 mg of total protein in 1 ml) were incubated with 1–2 µg of anti-WASH antibodies or control irrelevant IgGs (anti-GST) for 1 h at 4°C, and then protein G–Sepharose 4 Fast Flow (50 µl; GE Healthcare) was added and the incubation was continued for a further 2 h at 4°C. Beads were washed four times in lysis buffer and bound proteins were eluted in SDS sample buffer, separated by SDS-PAGE, and detected by immunoblotting with indicated antibodies using ECL Western Blotting Detection Reagents (GE Healthcare).

Fluorescent gelatin degradation assay

MDA-MB-231 cells were incubated for 5 h on FITC-conjugated cross-linked gelatin (Invitrogen) as described previously (Sakurai-Yageta et al., 2008), and then fixed and stained for F-actin and cortactin. Cells were imaged with the 63× objective of a wide-field microscope (DM6000 B/M; Leica) equipped with a CCD CoolSnap HQ camera (Roper Scientific) and steered by Metamorph (Molecular Devices). For quantification of degradation, the total area of degraded matrix in one field (black pixels) measured with the Threshold command of MetaMorph was divided by the number of phalloidin-labeled cells in the field to define a degradation index, which was normalized to the degradation index of control siNT-treated cells set to 100 as described previously (Sakurai-Yageta et al., 2008).

Indirect immunofluorescence microscopy, 3D deconvolution, and image analysis

MDA-MB-231 cells were cultured on gelatin-coated coverslips. Cells were extracted with 0.5% Triton X-100 in 4% paraformaldehyde and stained for immunofluorescence microscopy. Images were acquired with a wide-field microscope (Eclipse 90i Upright; Nikon) using a 100× Plan Apo VC 1.4 oil objective and a highly sensitive cooled interlined charge-coupled device (CCD) camera (CoolSnap HQ2; Roper Scientific). A z-dimension series of images was taken every 0.2 µm by means of a piezoelectric motor (Physik Instrumente) and the images were deconvoluted (Sibarita, 2005). For quantification of the effect of WASH knockdown on cortactin distribution, a perinuclear region was drawn with the Region Tool of MetaMorph 7 (Molecular Devices) and the integrated intensity was measured with the Region Measurement command. For quantification of the effect of Exo84 knockdown on WASH-cortactin domains, individual WASH and cortactin subdomains were circled with MetaMorph 7 and the integrated intensity was measured with the Region Measurement command.

WASH, Exo84, and cortactin spot detection and codistribution analysis

To detect endosomes, an automatic Otsu threshold is applied to the Gaussian-filtered MT1-MMP–positive endosome image (Σ = 1.5 pixels). Statistics about each endosome are then saved. For each endosome, WASH and Exo84 (or WASH and cortactin) spots are searched for in a neighboring of *x* pixels (manually set by user) in their respective channel. Their number and position are saved per endosome (see the macro in Text file S2 in online supplemental material). From the position of WASH and Exo84 (or WASH and cortactin) spots around each endosomes, each WASH spot is paired with its closest Exo84 (or cortactin) spot neighbor, optimized over all spots around this endosome. This allowed measuring of the distribution of distance between WASH-Exo84 (or WASH-cortactin) spots (see the codistribution analysis Zip file S3 in online supplemental material).

Duolink in situ proximity ligation assay

For Duolink assay (Söderberg et al., 2006), cells grown on coverslips coated with cross-linked gelatin were permeabilized with 0.5% Triton X-100 in 4% paraformaldehyde, fixed in 4% paraformaldehyde, and then incubated with primary antibodies: rabbit polyclonal anti-WASH, goat polyclonal anti-Exo84, and mouse monoclonal anti-cortactin. Secondary antibodies tagged with short DNA oligonucleotides were added. Hybridization, ligation, amplification, and detection were realized according to the manufacturer's protocol (Olink Bioscience). In brief, secondary antibodies were incubated in a preheated humidity chamber for 1 h at 37°C. Ligation was performed with a ligase-containing ligation solution for 30 min at 37°C. Then, the amplification step was performed with a polymerase-containing amplification solution for 1 h and 40 min at 37°C. Finally, coverslips were incubated with Cy3-conjugated IgGs to detect Duolink signal. Coverslips were analyzed by wide-field microscopy and WASH-Exo84 or WASH-cortactin Duolink signal staining was manually counted for each cell and compared with control conditions in which one of the primary antibodies was omitted.

Live-cell spinning disk confocal microscopy and FITC-dextran pulse experiment

MDA-MB-231 cells stably expressing MT1-MMPmCh were plated on glass-bottom dishes (MatTek Corporation) coated with cross-linked gelatin and kept in a humidified atmosphere at 37°C and 1% CO_2. Movement of MT1-MMPmCh–containing vesicles was monitored by acquiring z-stack sequences by confocal spinning disk microscopy (1 z-stack/4 s) with a microscope (Eclipse TE2000-U; Nikon) equipped with a 60× 1.45 NA oil immersion objective, a PIFOC Objective stepper, a CSU22 confocal unit (Yokogawa Corporation of America), and an HQ2 CCD camera steered by Metamorph and a temperature controller.

For dextran pulse experiments, MDA-MB-231 cells expressing MT1-MMPmCh (or transiently expressing Rab7-GFP or VAMP7-GFP) were plated in glass-bottom dishes coated with Alexa Fluor 594–conjugated cross-linked gelatin (or unlabeled gelatin) and a z-stack of images was acquired before adding dextran. FITC- or Alexa Fluor 647–conjugated dextran (10,000 MW) was added to the medium at 2 mg/ml final concentration (from a 20-mg/ml stock solution). After 1 min at 37°C, cells were washed and z-stack sequences were acquired.

TIRFM

MDA-MB-231 cells transfected with GFP- and mCherry-tagged proteins were plated on glass-bottom dishes coated with cross-linked unlabeled gelatin as previously described. Simultaneous dual color TIRFM sequences were acquired on an inverted microscope (TE2000) equipped with a 100× TIRF objective (1.47 NA), a TIRF arm, an image splitter (DV; Roper Scientific) installed in front of the CCD camera and a temperature controller. GFP and m-Cherry were excited with 491- and 560-nm lasers, respectively (100 mW; Roper Scientific), both controlled for power by an acousto-optic tunable filter. Fluorescent emissions were selected with bandpass and longpass filters (Chroma Technology Corp.) and captured by a QuantEM EMCCD camera (Roper Scientific). The system was driven by Metamorph. To measure the subplasma membrane density of MT1-MMP endosomes, cells stably expressing MT1-MMPmCh and silenced for the protein of interest were plated on a layer of unlabeled gelatin and imaged by TIRFM for an exposure time of 100 ms and with 1 pixel corresponding to 160 nm. The density of MT1-MMPmCh structures was evaluated by thresholding images using using ImageJ software. The threshold was set at 1.3× the cytoplasmic background. The size of the cell footprint was not affected by the siRNAs used.

High-resolution 3D structured illumination microscopy (SIM)

Image acquisition was performed in the 3D SIM mode with a N-SIM microscope (Nikon) equipped with a 100× 1.49 NA oil immersion objective, laser illumination (488 nm at 200 mW and 561 nm at 100 mW) and an EM CCD camera (DU-897; Andor Technology). Image reconstruction was performed using the NIS-Elements software (Nikon; based on Gustafsson et al. [2008]).

Matrigel and collagen I invasion assays

The Transwell Matrigel invasion assay has been previously described (Steffen et al., 2008). Invasive migration in 3D type I collagen was assessed using the Oris Cell Invasion Assay (Platypus Technologies). H2B-EGF–expressing MDA-MB-231 cells were reverse transfected with Lullaby reagent with MT1-MMP, WASH, or Exo84 siRNAs (50 nM). 24 h after transfection, cells were trypsinized and counted and 40,000 cells/well were seeded in the presence of Oris Cell Seeding Stoppers to restrict seeding to the outer annular regions of the wells in a 96-well plate previously coated with a bottom layer of acid-extracted rat tail tendon type I collagen (2.2 mg/ml; BD). Removal of the stoppers reveals a 2-mm diameter unseeded region in the center of each well, into which seeded cells may invade during a 48-h time period, once a collagen I overlay has been applied. H2B-EGFP nuclei images were acquired from each well at the beginning (T0) and 48 h after invasion (T2) using a cooled CCD camera (HQ2) mounted on a microscope (TE2000) equipped with a 4× objective CFI Plan Fluor 0.13 NA, 17.1 WD. Image analysis was performed using Metamorph software. The index of invasion was determined by thresholding the area occupied by H2B-EGFP nuclei in the detection zone of each well after 48 h of invasion. This index is defined by the total area occupied by H2B-EGFP nuclei in unseeded area at the end of the assay (T2) by subtracting the area occupied by H2B-EGFP nuclei at the beginning of the experiment (T0). This area of invasion was normalized and results from three independent experiments are represented.

Live-cell imaging of cells on a layer of fibrous type I collagen

Glass bottom dishes (MatTek Corporation) were layered with 100 µl of a solution of type I collagen mixed with Alexa Fluor 647–conjugated type I collagen (10% final) at a final concentration of 2.2 mg/ml (Sabeh et al., 2004). After gelling for 3 min at 37°C, the collagen layer was washed gently in PBS and 1 ml of the cell suspension in L15 medium with 15% FCS ($1.5–2.5 \times 10^5$ cells/ml) was added. Cells were incubated for 30 min at 37°C in 1% CO_2 before live-cell imaging using multi-color spinning disk confocal microscopy.

Quantification of pericellular collagenolysis

Cells treated with siRNAs against MT1-MMP, WASH, Exo84, or non-targeting siRNA for 48 h (Table S2) were trypsinized and resuspended in 0.2 ml of 2.2 mg/ml collagen I solution (2.5×10^5 cells/ml) loaded on a glass coverslip. After gelling for 30 min at 37°C, complete medium was added and collagen-embedded cells were incubated for 24 h at 37°C in 1% CO_2. After fixation in 4% paraformaldehyde in PBS at 37°C for 30 min, samples were incubated with anti–Col1-$^{3/4}$C antibodies (2.5 µg/ml) for 2 h at 4°C, washed extensively with PBS, and counterstained with Cy3-conjugated anti-rabbit IgG antibodies, DAPI, and Alexa Fluor 488–phalloidin to see the cell shape. Image acquisition was performed with an A1R confocal microscope (Nikon) with a 40× oil objective. Quantification of degradation spots was performed with a homemade ImageJ macro (Zip file S1 in the online supplemental material). Images were preprocessed by a laplacian of Gaussian filter (Sage et al., 2005), with variance reflecting the expected spot size. The spot detection then consists in finding the local minima, sorting them in ascending order of intensity, applying a flood-fill algorithm to each of them using a fixed noise tolerance value set up for all experiments at 10,000, and discarding higher minima whose fill regions touch those of lower minima. Detected spots are then counted and saved for visual verification. No manual correction was done. Degradation index is the number of degradation spots divided by the number of cells present in the field, normalized to the degradation index of control cells set to 100.

MT1-MMPpHluorin exocytosis on collagen type I fibers

MDA-MB-231 cells stably coexpressing MT1-MMPmCherry and MT1-MMPpHluorin constructs were treated with nontargeting, WASH, or Exo84 siRNA for 72 h and plated atop of a drop of polymerized type I collagen. Cells were imaged by confocal spinning disk microscopy (two images/min). The number of exocytic events of MT1-MMPphLuorin (i.e., GFP flashes) was measured per minute and per cell. As a control we measured the mean fluorescence intensity of MT1-MMPmCherry for each cell.

Extracellular pH shifts experiment

MDA-MB-231 cells stably expressing MT1-MMPpHluorin were plated on polymerized type I collagen conjugated with Cy3. Cells were imaged on a microsope (IX71; Olympus) with a 100×, 1.49 NA objective at a frame rate of 0.5 Hz with a QuantEM EMCCD camera. Cells were bathed in a solution containing 140 mM NaCl, 2 mM KCl, 2 mM $MgCl_2$, 2 mM $CaCl_2$, 10 mM Hepes, and 5 mM D-glucose, and adjusted to pH 7.4 and 315 mosm. For the solution at pH 5.5, Hepes was replaced by MES. Solution exchange was performed as described previously (Perrais et al., 2004).

Statistical analyses

Statistical analyses were performed using analysis of variance or Student's *t* test in Prism software.

Online supplemental material

Fig. S1 shows additional data on markers associated with MT1-MMP–positive endosomes in MDA-MB-231 and BT-549 cells. Fig. S2 shows levels of proteins in cells targeted by different siRNAs. Fig. S3 shows additional staining of endosomal and invadopodial markers. Fig. S4 shows a gallery of images taken from a time-lapse sequence of cells expressing MT1-MMPmCh and MT1-MMPpHLuorin. Tables S1 and S2 list antibodies and show sequences of the siRNAs used in this study, respectively. Video 1 shows the dynamics of GFP-WASH– and DsRed-cortactin–positive cytoplasmic puncta in MDA-MB-231 cells. Video 2 shows clustering and tubulation of a MT1-MMP–positive late endosomal system induced upon silencing of WASH in MDA-MB-231 cells. Video 3 dynamically shows contacts of MT1-MMPmCherry–positive endosomes with GFP-cortactin–positive invadopodia on the ventral membrane of MDA-MB-231 cells plated on gelatin. Video 4 documents the existence of two dynamic pools of DsRed-cortactin in MDA-MB-231 cells plated on a layer of collagen fibers; one pool assembles along collagen fibers and correspond to linear invadopodia, and another pool is associated with GFP-WASH–positive puncta on late endosomes. Video 5 shows MDA-MB-231 cells simultaneously expressing mCherry- and pHLuorin-tagged fusion protein of MT1-MMP plated on a layer of collagen fibers. The pH sensitivity of pHLuorin allows the visualization of exocytic events of MT1-MMP–containing endosomes occurring near collagen fibers. Video 6 documents that exocytic MT1-MMPpHLuorin–positive endosomes are positive for mCherry-WASH. Video 7 shows the fluorescence change of MT1-MMPpHLuorin–containing late endosomes according to the pH of the external medium indicative of long-lived late endosome-to-plasma membrane connections. Zip file S1 contains two macros: one for degradation spot detection and one for DAPI-stained nuclei counting, to compute the degradation index of collagen. Text file S2 is the macro used to detect endosomes and aggregated spots. Zip file S3 (codistribution analysis) contains Matlab scripts used to quantify the distance between WASH spots and their closest neighbored cortactin spots (or Exo84 spots) for each endosome. Online supplemental material is available at http://www.jcb.org/cgi/content/full/jcb.201306162/DC1.

The authors wish to thank J. Camonis for initiating the Drosoman yeast two-hybrid joint project between Institut Curie and Hybrigenics SA, A. Savina for help with FITC-dextran experiments, and K. Wolf and P. Friedl for advice and help with experiments using Col1-$^{3/4}$C antibody. We are indebted to V. Fraisier and the staff of the Cell and Tissue Imaging Facility and Nikon Imaging Center at Institut Curie–Centre National de la Recherche Scientifique for help with image acquisition. We thank members of P. Chavrier's laboratory for helpful discussions.

P. Monteiro was the recipient of a PhD fellowship from Ligue Nationale contre le Cancer. C. Rossé was the recipient of a postdoctoral fellowship from Fondation ARC pour la recherche sur le cancer. Support was provided by grants from the Fondation ARC pour la recherche sur le cancer (SL220100601356) and Agence Nationale pour la Recherche (ANR-08-BLAN-0111) to P. Chavrier, by GenHomme Network (02490-6088) to Hybrigenics SA and to Institut Curie, and by core funding from the Institut Curie and the Centre National de la Recherche Scientifique.

Submitted: 28 June 2013
Accepted: 18 November 2013

References

Artym, V.V., Y. Zhang, F. Seillier-Moiseiwitsch, K.M. Yamada, and S.C. Mueller. 2006. Dynamic interactions of cortactin and membrane type 1 matrix metalloproteinase at invadopodia: defining the stages of invadopodia formation and function. *Cancer Res.* 66:3034–3043. http://dx.doi.org/10.1158/0008-5472.CAN-05-2177

Ayala, I., M. Baldassarre, G. Giacchetti, G. Caldieri, S. Tetè, A. Luini, and R. Buccione. 2008. Multiple regulatory inputs converge on cortactin to control invadopodia biogenesis and extracellular matrix degradation. *J. Cell Sci.* 121:369–378. http://dx.doi.org/10.1242/jcs.008037

Bartel, P.L., C.T. Chien, R. Sternglanz, and S. Fields. 1993. Using the two-hybrid system to detect protein-protein interactions. *In* Cellular Interactions in Development: A Practical Approach, D.A. Hartley, editor. Oxford University Press, Oxford. 153–179.

Carnell, M., T. Zech, S.D. Calaminus, S. Ura, M. Hagedorn, S.A. Johnston, R.C. May, T. Soldati, L.M. Machesky, and R.H. Insall. 2011. Actin polymerization driven by WASH causes V-ATPase retrieval and vesicle neutralization before exocytosis. *J. Cell Biol.* 193:831–839. http://dx.doi.org/10.1083/jcb.201009119

Clark, E.S., A.S. Whigham, W.G. Yarbrough, and A.M. Weaver. 2007. Cortactin is an essential regulator of matrix metalloproteinase secretion and extracellular matrix degradation in invadopodia. *Cancer Res.* 67:4227–4235. http://dx.doi.org/10.1158/0008-5472.CAN-06-3928

Derivery, E., C. Sousa, J.J. Gautier, B. Lombard, D. Loew, and A. Gautreau. 2009. The Arp2/3 activator WASH controls the fission of endosomes through a large multiprotein complex. *Dev. Cell*. 17:712–723. http://dx.doi.org/10.1016/j.devcel.2009.09.010

Derivery, E., E. Helfer, V. Henriot, and A. Gautreau. 2012. Actin polymerization controls the organization of WASH domains at the surface of endosomes. *PLoS ONE*. 7:e39774. http://dx.doi.org/10.1371/journal.pone.0039774

Duleh, S.N., and M.D. Welch. 2010. WASH and the Arp2/3 complex regulate endosome shape and trafficking. *Cytoskeleton (Hoboken)*. 67:193–206.

Fromont-Racine, M., J.C. Rain, and P. Legrain. 1997. Toward a functional analysis of the yeast genome through exhaustive two-hybrid screens. *Nat. Genet.* 16:277–282. http://dx.doi.org/10.1038/ng0797-277

Gomez, T.S., and D.D. Billadeau. 2009. A FAM21-containing WASH complex regulates retromer-dependent sorting. *Dev. Cell*. 17:699–711. http://dx.doi.org/10.1016/j.devcel.2009.09.009

Gomez, T.S., J.A. Gorman, A.A. de Narvajas, A.O. Koenig, and D.D. Billadeau. 2012. Trafficking defects in WASH-knockout fibroblasts originate from collapsed endosomal and lysosomal networks. *Mol. Biol. Cell*. 23:3215–3228. http://dx.doi.org/10.1091/mbc.E12-02-0101

Gustafsson, M.G., L. Shao, P.M. Carlton, C.J. Wang, I.N. Golubovskaya, W.Z. Cande, D.A. Agard, and J.W. Sedat. 2008. Three-dimensional resolution doubling in wide-field fluorescence microscopy by structured illumination. *Biophys. J.* 94:4957–4970. http://dx.doi.org/10.1529/biophysj.107.120345

Harrington, A.W., C. St Hillaire, L.S. Zweifel, N.O. Glebova, P. Philippidou, S. Halegoua, and D.D. Ginty. 2011. Recruitment of actin modifiers to TrkA endosomes governs retrograde NGF signaling and survival. *Cell*. 146:421–434. http://dx.doi.org/10.1016/j.cell.2011.07.008

He, B., and W. Guo. 2009. The exocyst complex in polarized exocytosis. *Curr. Opin. Cell Biol.* 21:537–542. http://dx.doi.org/10.1016/j.ceb.2009.04.007

Heider, M.R., and M. Munson. 2012. Exorcising the exocyst complex. *Traffic*. 13:898–907. http://dx.doi.org/10.1111/j.1600-0854.2012.01353.x

Hertzog, M., and P. Chavrier. 2011. Cell polarity during motile processes: keeping on track with the exocyst complex. *Biochem. J.* 433:403–409. http://dx.doi.org/10.1042/BJ20101214

Hotary, K., X.Y. Li, E. Allen, S.L. Stevens, and S.J. Weiss. 2006. A cancer cell metalloprotease triad regulates the basement membrane transmigration program. *Genes Dev.* 20:2673–2686. http://dx.doi.org/10.1101/gad.1451806

Jia, D., T.S. Gomez, Z. Metlagel, J. Umetani, Z. Otwinowski, M.K. Rosen, and D.D. Billadeau. 2010. WASH and WAVE actin regulators of the Wiskott-Aldrich syndrome protein (WASP) family are controlled by analogous structurally related complexes. *Proc. Natl. Acad. Sci. USA*. 107:10442–10447. http://dx.doi.org/10.1073/pnas.0913293107

Jiang, A., K. Lehti, X. Wang, S.J. Weiss, J. Keski-Oja, and D. Pei. 2001. Regulation of membrane-type matrix metalloproteinase 1 activity by dynamin-mediated endocytosis. *Proc. Natl. Acad. Sci. USA*. 98:13693–13698. http://dx.doi.org/10.1073/pnas.241293698

Juin, A., C. Billottet, V. Moreau, O. Destaing, C. Albiges-Rizo, J. Rosenbaum, E. Génot, and F. Saltel. 2012. Physiological type I collagen organization induces the formation of a novel class of linear invadosomes. *Mol. Biol. Cell*. 23:297–309. http://dx.doi.org/10.1091/mbc.E11-07-0594

Kerrien, S., B. Aranda, L. Breuza, A. Bridge, F. Broackes-Carter, C. Chen, M. Duesbury, M. Dumousseau, M. Feuermann, U. Hinz, et al. 2012. The IntAct molecular interaction database in 2012. *Nucleic Acids Res.* 40:D841–D846. http://dx.doi.org/10.1093/nar/gkr1088

Liu, J., P. Yue, V.V. Artym, S.C. Mueller, and W. Guo. 2009. The role of the exocyst in matrix metalloproteinase secretion and actin dynamics during tumor cell invadopodia formation. *Mol. Biol. Cell*. 20:3763–3771. http://dx.doi.org/10.1091/mbc.E08-09-0967

Lizárraga, F., R. Poincloux, M. Romao, G. Montagnac, G. Le Dez, I. Bonne, G. Rigaill, G. Raposo, and P. Chavrier. 2009. Diaphanous-related formins are required for invadopodia formation and invasion of breast tumor cells. *Cancer Res.* 69:2792–2800. http://dx.doi.org/10.1158/0008-5472.CAN-08-3709

Lorenz, M., H. Yamaguchi, Y. Wang, R.H. Singer, and J. Condeelis. 2004. Imaging sites of N-wasp activity in lamellipodia and invadopodia of carcinoma cells. *Curr. Biol.* 14:697–703. http://dx.doi.org/10.1016/j.cub.2004.04.008

Miesenböck, G. 2012. Synapto-pHluorins: genetically encoded reporters of synaptic transmission. *Cold Spring Harb. Protoc*. 2012:213–217. http://dx.doi.org/10.1101/pdb.ip067827

Morel, E., R.G. Parton, and J. Gruenberg. 2009. Annexin A2-dependent polymerization of actin mediates endosome biogenesis. *Dev. Cell*. 16:445–457. http://dx.doi.org/10.1016/j.devcel.2009.01.007

Murphy, D.A., and S.A. Courtneidge. 2011. The 'ins' and 'outs' of podosomes and invadopodia: characteristics, formation and function. *Nat. Rev. Mol. Cell Biol.* 12:413–426. http://dx.doi.org/10.1038/nrm3141

Oser, M., H. Yamaguchi, C.C. Mader, J.J. Bravo-Cordero, M. Arias, X. Chen, V. Desmarais, J. van Rheenen, A.J. Koleske, and J. Condeelis. 2009. Cortactin regulates cofilin and N-WASp activities to control the stages of invadopodium assembly and maturation. *J. Cell Biol.* 186:571–587. http://dx.doi.org/10.1083/jcb.200812176

Oser, M., C.C. Mader, H. Gil-Henn, M. Magalhaes, J.J. Bravo-Cordero, A.J. Koleske, and J. Condeelis. 2010. Specific tyrosine phosphorylation sites on cortactin regulate Nck1-dependent actin polymerization in invadopodia. *J. Cell Sci.* 123:3662–3673. http://dx.doi.org/10.1242/jcs.068163

Park, L., P.A. Thomason, T. Zech, J.S. King, D.M. Veltman, M. Carnell, S. Ura, L.M. Machesky, and R.H. Insall. 2013. Cyclical action of the WASH complex: FAM21 and capping protein drive WASH recycling, not initial recruitment. *Dev. Cell*. 24:169–181. http://dx.doi.org/10.1016/j.devcel.2012.12.014

Perrais, D., I.C. Kleppe, J.W. Taraska, and W. Almers. 2004. Recapture after exocytosis causes differential retention of protein in granules of bovine chromaffin cells. *J. Physiol.* 560:413–428. http://dx.doi.org/10.1113/jphysiol.2004.064410

Piotrowski, J.T., T.S. Gomez, R.A. Schoon, A.K. Mangalam, and D.D. Billadeau. 2013. WASH knockout T cells demonstrate defective receptor trafficking, proliferation, and effector function. *Mol. Cell. Biol.* 33:958–973. http://dx.doi.org/10.1128/MCB.01288-12

Poincloux, R., F. Lizárraga, and P. Chavrier. 2009. Matrix invasion by tumour cells: a focus on MT1-MMP trafficking to invadopodia. *J. Cell Sci.* 122:3015–3024. http://dx.doi.org/10.1242/jcs.034561

Puthenveedu, M.A., B. Lauffer, P. Temkin, R. Vistein, P. Carlton, K. Thorn, J. Taunton, O.D. Weiner, R.G. Parton, and M. von Zastrow. 2010. Sequence-dependent sorting of recycling proteins by actin-stabilized endosomal microdomains. *Cell*. 143:761–773. http://dx.doi.org/10.1016/j.cell.2010.10.003

Rowe, R.G., and S.J. Weiss. 2008. Breaching the basement membrane: who, when and how? *Trends Cell Biol.* 18:560–574. http://dx.doi.org/10.1016/j.tcb.2008.08.007

Sabeh, F., I. Ota, K. Holmbeck, H. Birkedal-Hansen, P. Soloway, M. Balbin, C. Lopez-Otin, S. Shapiro, M. Inada, S. Krane, et al. 2004. Tumor cell traffic through the extracellular matrix is controlled by the membrane-anchored collagenase MT1-MMP. *J. Cell Biol.* 167:769–781. http://dx.doi.org/10.1083/jcb.200408028

Sabeh, F., R. Shimizu-Hirota, and S.J. Weiss. 2009. Protease-dependent versus -independent cancer cell invasion programs: three-dimensional amoeboid movement revisited. *J. Cell Biol.* 185:11–19. http://dx.doi.org/10.1083/jcb.200807195

Sage, D., F.R. Neumann, F. Hediger, S.M. Gasser, and M. Unser. 2005. Automatic tracking of individual fluorescence particles: application to the study of

chromosome dynamics. *IEEE Trans. Image Process.* 14:1372–1383. http://dx.doi.org/10.1109/TIP.2005.852787

Sakurai-Yageta, M., C. Recchi, G. Le Dez, J.B. Sibarita, L. Daviet, J. Camonis, C. D'Souza-Schorey, and P. Chavrier. 2008. The interaction of IQGAP1 with the exocyst complex is required for tumor cell invasion downstream of Cdc42 and RhoA. *J. Cell Biol.* 181:985–998. http://dx.doi.org/10.1083/jcb.200709076

Sibarita, J.B. 2005. Deconvolution microscopy. *Adv. Biochem. Eng. Biotechnol.* 95:201–243.

Söderberg, O., M. Gullberg, M. Jarvius, K. Ridderstråle, K.J. Leuchowius, J. Jarvius, K. Wester, P. Hydbring, F. Bahram, L.G. Larsson, and U. Landegren. 2006. Direct observation of individual endogenous protein complexes in situ by proximity ligation. *Nat. Methods*. 3:995–1000. http://dx.doi.org/10.1038/nmeth947

Sokac, A.M., and W.M. Bement. 2006. Kiss-and-coat and compartment mixing: coupling exocytosis to signal generation and local actin assembly. *Mol. Biol. Cell*. 17:1495–1502. http://dx.doi.org/10.1091/mbc.E05-10-0908

Steffen, A., G. Le Dez, R. Poincloux, C. Recchi, P. Nassoy, K. Rottner, T. Galli, and P. Chavrier. 2008. MT1-MMP-dependent invasion is regulated by TI-VAMP/VAMP7. *Curr. Biol.* 18:926–931. http://dx.doi.org/10.1016/j.cub.2008.05.044

Temkin, P., B. Lauffer, S. Jäger, P. Cimermancic, N.J. Krogan, and M. von Zastrow. 2011. SNX27 mediates retromer tubule entry and endosome-to-plasma membrane trafficking of signalling receptors. *Nat. Cell Biol.* 13:715–721. http://dx.doi.org/10.1038/ncb2252

Thorn, P., K.E. Fogarty, and I. Parker. 2004. Zymogen granule exocytosis is characterized by long fusion pore openings and preservation of vesicle lipid identity. *Proc. Natl. Acad. Sci. USA*. 101:6774–6779. http://dx.doi.org/10.1073/pnas.0400336101

Uekita, T., Y. Itoh, I. Yana, H. Ohno, and M. Seiki. 2001. Cytoplasmic tail–dependent internalization of membrane-type 1 matrix metalloproteinase is important for its invasion-promoting activity. *J. Cell Biol.* 155:1345–1356. http://dx.doi.org/10.1083/jcb.200108112

Vojtek, A.B., and S.M. Hollenberg. 1995. Ras-Raf interaction: two-hybrid analysis. *Methods Enzymol.* 255:331–342.

Williams, K.C., and M.G. Coppolino. 2011. Phosphorylation of membrane type 1-matrix metalloproteinase (MT1-MMP) and its vesicle-associated membrane protein 7 (VAMP7)-dependent trafficking facilitate cell invasion and migration. *J. Biol. Chem.* 286:43405–43416. http://dx.doi.org/10.1074/jbc.M111.297069

Wolf, K., Y.I. Wu, Y. Liu, J. Geiger, E. Tam, C. Overall, M.S. Stack, and P. Friedl. 2007. Multi-step pericellular proteolysis controls the transition from individual to collective cancer cell invasion. *Nat. Cell Biol.* 9:893–904. http://dx.doi.org/10.1038/ncb1616

Yamaguchi, H., M. Lorenz, S. Kempiak, C. Sarmiento, S. Coniglio, M. Symons, J. Segall, R. Eddy, H. Miki, T. Takenawa, and J. Condeelis. 2005. Molecular mechanisms of invadopodium formation: the role of the N-WASP–Arp2/3 complex pathway and cofilin. *J. Cell Biol.* 168:441–452. http://dx.doi.org/10.1083/jcb.200407076

Yu, X., T. Zech, L. McDonald, E.G. Gonzalez, A. Li, I. Macpherson, J.P. Schwarz, H. Spence, K. Futó, P. Timpson, et al. 2012. N-WASP coordinates the delivery and F-actin–mediated capture of MT1-MMP at invasive pseudopods. *J. Cell Biol.* 199:527–544. http://dx.doi.org/10.1083/jcb.201203025

Zech, T., S.D. Calaminus, P. Caswell, H.J. Spence, M. Carnell, R.H. Insall, J. Norman, and L.M. Machesky. 2011. The Arp2/3 activator WASH regulates α5β1-integrin-mediated invasive migration. *J. Cell Sci.* 124:3753–3759. http://dx.doi.org/10.1242/jcs.080986